Minlo t-channel single-top plus jet

Stefano Carrazza,[a] **Rikkert Frederix,**[b] **Keith Hamilton**[a,c] **and Giulia Zanderighi**[a,1]

[a] *CERN, Theoretical Physics Department, CH-1211,*
  Geneva 23, Switzerland

[b] *Physik Department T31, Technische Universität München,*
  James-Franck-Str. 1, 85748 Garching, Germany

[c] *Department of Physics and Astronomy, University College London,*
  London, WC1E 6BT, U.K.

  E-mail: stefano.carrazza@cern.ch, rikkert.frederix@tum.de,
  keith.hamilton@ucl.ac.uk, giulia.zanderighi@cern.ch

Abstract: We present a next-to-leading order accurate simulation of t-channel single-top plus jet production matched to parton showers via the Powheg method. The calculation underlying the simulation is enhanced with a process-specific implementation of the multi-scale improved NLO (Minlo) method, such that it gives physical predictions all through phase space, including regions where the jet additional to the t-channel single-top process is unresolved. We further describe a tuning procedure for the Minlo Sudakov form factor, fitting the coefficient of the first subleading term in its exponent using an artificial neural-network. The latter tuning, implemented as a straightforward event-by-event reweighting, renders the Minlo simulation NLO accurate for t-channel single-top observables, in addition to those of the analogous single-top plus jet process.

---

[1]On leave from: Rudolf Peierls Centre for Theoretical, Physics, 1 Keble Road, University of Oxford, Oxford, U.K.

Contents

1 Introduction

The top quark is the heaviest of all the known elementary particles. Owing to the closeness of its mass to the electroweak scale, and its large Yukawa coupling to the Higgs boson, the top quark is considered to have a special role in, and be a sensitive probe of, both the mechanism of electroweak symmetry breaking [1, 2] and physics beyond the standard model. The top is further unique among the quarks insofar as it predominantly decays before hadronizing. This fact implies that one can explore the electroweak properties of a bare quark [3].

At the LHC the production rate of top quarks is large. For *pp* collisions at 13 TeV centre-of-mass energy, with a top mass of 172.5 GeV, the main channel, top pair-production,

is predicted to have a cross section of 832^{+40}_{-46} pb [4–7]. Hence, by the end of Run II of the LHC, later this year, 100 million top pairs will have been produced by this mechanism. These very large event samples facilitate precise measurements of fundamental top-quark properties, such as its mass and its couplings to other standard model particles.

The second largest mechanism for the production of top quarks at the LHC is through electroweak single-top production, in which a down-type quark — typically the bottom quark — is converted to a top quark by interacting with a W-boson. The cross section for this process is very close to being one third that of top-quark pair production at the 13 TeV LHC [8–11]. Despite being a slightly less copious source of top quarks and a difficult reaction to analyse from an experimental perspective, single-top production is nevertheless a uniquely interesting process to study. Perhaps most notably it provides a means to directly measure the Cabibbo-Kobayashi-Maskawa (CKM) matrix element $|V_{tb}|$, which is otherwise only measured indirectly [12–15]. Additionally, in numerous beyond the standard model scenarios, single-top production provides a more sensitive probe of new physics than other processes [16–21]. Finally, besides being an interesting process in its own right, it is also important to have a detailed understanding of single-top production in order to control it as a background in other standard model analyses and new physics searches, e.g. standard model Higgs production in association with a W-boson.

Single-top production is usually classified in three separate modes, based on the virtuality of the participating W-boson. The t-channel mechanism, where the W-boson has a negative virtuality, has the largest cross section at the LHC. This is followed by the associated Wt production mode, where the virtuality of the W-boson is zero, whose cross section is three to four times smaller than that of the t-channel process, for centre-of-mass energies in the range $7 - 14$ TeV. The s-channel production mode, in which the W-boson has positive virtuality, has the lowest rate of all three single-top channels, being up to a factor of ten smaller than the Wt channel at the LHC.[1] In this work we concentrate on the dominant mode, namely, t-channel single-top production.

Experimental analysis of t-channel single-top production is particularly difficult at the LHC due to the large background from $t\bar{t}$ and W+jets events. Even so, this process has been measured and studied by both ATLAS [22–27] and CMS [28–34] at 7, 8 and 13 TeV. For recent reviews on experimental studies of single-top production both at the Tevatron and LHC see refs. [35, 36].

On the theoretical front, predictions for hadronic single-top production processes in the framework of fixed order perturbative QCD have also been a subject of considerable work and progress. t-channel single-top production has been computed at next-to-leading order (NLO) in QCD perturbation theory, including NLO corrections to the top-quark decays, in refs. [37–39]. These calculations were carried out in the so-called five-flavour scheme, in which the b-quark is treated in the massless approximation. More recently, NLO accurate calculations were carried out and implemented in the MCFM Monte Carlo package in the four flavour scheme [40, 41] — wherein the b-quark is instead treated as

---

[1]At higher orders in perturbation theory these production modes interfere, this is discussed in detail in section 2.1.

a massive parton — including spin correlations, in the zero-width approximation, for the top-quark decays [42]. Ground-breaking work in the last four years has seen the accuracy of fixed order perturbative predictions for t-channel single-top production further extended to next-to-next-to-leading order (NNLO) [43–45], in the approximation in which one neglects $\mathcal{O}(\alpha_\text{s}^2)$ colour suppressed interference terms.

Beyond fixed order perturbation theory, all orders analytic resummation of threshold logarithms has been presented in refs. [46, 47], with transverse momentum resummation effects having been studied in ref. [48]. Precision Monte Carlo simulations of t-channel single-top production processes have also been developed, based on the matching of NLO calculations with parton showers (Nlops), in the MC@NLO [49–51], Powheg [51, 52], and Sherpa [53] frameworks.

Off-shell top-quark effects have also been considered at NLO, both at fixed order [54, 55] and further in the context of NLO parton shower matched simulations [56–58]. These studies reveal such effects to be small away from kinematic end-points. Finally, electroweak corrections to t-channel single-top production have been computed and also found to be small [59–61], affecting the total cross section at the sub-percent level, but with the effects rising in regions where the kinematic invariants associated with the process become large.

While the Nlops Monte Carlo description of single-top production reaches a remarkable level of accuracy and sophistication, it is not as advanced as that afforded to other processes, such as Higgs, W-, and Z-boson production. In particular, powerful methods recently developed for merging together Nlops simulations of processes that differ only in their jet multiplicity [62–71], e.g. Higgs and Higgs plus jet production simulations, have not so far been applied to single-top. With the exception of relative $\mathcal{O}(\alpha_s^2)$ virtual corrections, event generators based on these methods contain all of the same fixed order information as found in NNLO calculations, all consistently matched to leading-log parton shower resummation and tuned non-perturbative models.

In the present work, we constructed a first Nlops simulation of t-channel single-top plus jet production within the Powheg Box framework [72, 73], with matrix elements obtained from MadGraph5_aMC@NLO and related packages [74–78]. We then enhanced the underlying NLO calculation according to the multiscale improved NLO (Minlo) procedure [63], with important but straightforward specializations to the case at hand. Finally, we have invoked the basic idea put forward in ref. [79], with substantial refinements and extensions, to recover NLO accuracy in the lower multiplicity t-channel single-top process, by approximately fitting unknown, subleading, $\mathcal{O}(\alpha_\text{s}^2)$ terms in the Minlo Sudakov form factor. In particular, to tune the latter Sudakov form factor we make use of machine learning methods in the form of an artificial neural network.

Formally, the minimal, sufficient condition for carrying out tuning to this effect is merely that, beforehand, the Minlo t-channel single-top plus jet computation must be at least LO accurate for inclusive t-channel single-top production observables. This is implicitly the case if the resummation formula underlying the initial Minlo simulation is

next-to-leading-log (NLL_σ) accurate, as in this work.[2] If the latter condition is satisfied, the desired NLO corrections to inclusive t-channel single-top observables can be accounted for by introducing a $\mathcal{O}(\text{NNLL}_\sigma)$ term in the MINLO Sudakov form factor, with a fitted $\mathcal{O}(1)$ coefficient. This is a straightforward mathematical fact, that need not have anything to do with resummation. The tuning procedure will raise the MINLO t-channel single-top plus jet description of inclusive t-channel single-top observables to NLO accuracy by construction. At the same time, since this is achieved by introducing only a $\mathcal{O}(\text{NNLL}_\sigma)$ term in the MINLO Sudakov exponent, the NLO accuracy already in place for t-channel single-top plus jet production will remain intact.

Introducing higher order terms in Sudakov form factors, to unitarize cross sections, be they spurious or not, is not new. For example, the H/W/ZJ-MINLO$'$ simulations of ref. [69], achieving the same level of accuracy that we aim for in this work, have this property. The H/W/ZJ-MINLO$'$ constructions eliminated $\mathcal{O}(\alpha_{\text{S}}^{3/2})$ differences between H/W/ZJ-MINLO predictions for inclusive observables and conventional NLO ones, by adding $\mathcal{O}(\text{N}^3\text{LL}_\sigma)$, '$B_2$', terms in the MINLO Sudakov form factor. While inclusion of the latter 'B_2' terms led to the desired level of fixed order accuracy, their inclusion is completely spurious from the point of view of resummation: the resummation accuracy associated to those simulations before and after inclusion of the 'B_2' terms is completely unchanged. This owes to the fact that the resummation formula underlying those simulations is based on resumming the H/W/Z transverse momentum spectrum directly in transverse momentum space.

As already stated above, to reach our (fixed order) accuracy goals, we are only required to control terms at the NLL_σ level in the MINLO resummation formula prior to invoking the tuning procedure: we do not require any information on the form, or ingredients, of a more accurate formula for this aim. Nevertheless, we postulate that the only difference between the *form* of our NLL_σ MINLO resummation formula and its NNLL_σ extension, merely lies in the inclusion of a NNLL_σ term in the Sudakov form factor. Thus, while it is unnecessary for achieving our desired level of fixed order accuracy, if our mild postulate on the form of the NNLL_σ resummation formula holds, when rendering MINLO t-channel single-top plus jet NLO accurate for inclusive t-channel single-top observables, we will implicitly also improve the NLL_σ MINLO resummation towards the true NNLL_σ result.

In section 2 we present the theoretical framework, charting the construction of our simulation: first the NLO computation, followed by its MINLO extension, and on to the tuning of the latter Sudakov form factor. In section 3 we validate the t-channel single-top MINLO simulation, STJ, and its tuned counterpart, STJ*, by comparing their predictions to one another, as well as to those of the lower multiplicity POWHEG t-channel single-top production code, ST [52]. We conclude in section 4. Finally, appendix A provides supplementary details on the theoretical framework, while additional numerical results are given in appendix B, to give insight on the robustness of the tuning in the STJ* simulation.

---

[2]NLL_σ resummation controls all terms in the t-channel single-top plus jet cross section $\propto \frac{1}{y_{12}} \bar{\alpha}_{\text{S}}^n \ln^m \frac{Q^2}{y_{12}}$, with $m = 2n-1$ and $m = 2n-2$, wherein Q is a scale characteristic of the hard, underlying, $2 \to 2$ scattering, and y_{12} is the value of the distance measure in the exclusive k_t clustering algorithm [80], where a single-top plus jet event is resolved as a single-top one. NNLL_σ resummation also controls $m = 2n - 3$ terms.

2 Theoretical framework

In this section we describe the main elements of our t-channel single-top plus jet simulation and their connections. In section 2.1 we give details on the precise definition of the t-channel single-top process, addressing issues that arise there due to ambiguities at $\mathcal{O}(\alpha_s^2)$. Section 2.2 documents the matrix elements used in building our initial NLOPS t-channel single-top plus jet simulation, and its assembly in the POWHEG BOX framework. The enhancement of the latter with a process-specific adaptation of the multi-scale improved NLO (MINLO) method is described in section 2.3. In section 2.4 we describe how one can tune the Sudakov form factor in the latter STJ simulation such that it recovers NLO accurate predictions for inclusive t-channel single-top production observables, while retaining NLO accuracy for single-top plus jet ones. Section 2.5 goes on to describe a concrete realization of this method, making use of machine learning algorithms.

For brevity, throughout our work, we will refer to the inclusive t-channel single-top process as ST, and the t-channel single-top plus jet process as STJ. The abbreviation ST will be further used to denote the POWHEG inclusive t-channel single-top production program [52], which is NLO accurate in the description of inclusive t-channel single-top observables. Similarly, we will use STJ to refer to our MINLO t-channel single-top plus jet simulation, NLO accurate in the description of STJ observables. The tuned counterpart of STJ is labelled STJ*.

2.1 Process definition

We consider the t-channel single-top production process in the five-flavour scheme, wherein, at the lowest order in perturbation theory, a massless initial state bottom quark is converted to a top quark through the exchange of a t-channel, space-like W-boson. The W-boson is also connected to another quark line, in which an initial state up-type quark (down-type anti-quark) from the first two generations is converted to a final state down-type quark (up-type anti-quark), again from the first two generations. We refer to these quark lines as the *heavy quark line* and the *light quark line*, respectively.

To NLO in perturbation theory, $\mathcal{O}(\alpha_s)$, radiative corrections to t-channel single-top production factorise exactly into independent corrections to the heavy and light quark lines, respectively. Moreover, to NLO, t-channel single-top production does not interfere with other single-top production modes. On the other hand, when considering $\mathcal{O}(\alpha_s^2)$ terms, as in NLO t-channel single-top plus jet production, contributions to the cross section start to arise from interference between radiative corrections to the heavy and light quark lines. Since the heavy and light quark lines correspond to two different colour lines, interference of their associated radiative corrections amounts to an interference of colour structures. Correspondingly, such $\mathcal{O}(\alpha_s^2)$ contributions are suppressed by at least two powers of the number of colours, $N_c = 3$, relative to those involving no dynamical correlation between the heavy and light quark lines [43–45]. A non-zero interference of s- and t-channel single-top production modes is also understood to develop at $\mathcal{O}(\alpha_s^2)$ [45].

The goal of this work is to construct a simulation which is NLO accurate in the description of t-channel single-top and t-channel single-top plus jet production. For the

former, $\mathcal{O}(\alpha_{\rm s}^2)$ terms do not contribute to NLO. Taking the latter point together with the expectation that the aforementioned $\mathcal{O}(\alpha_{\rm s}^2)$ colour suppressed interference terms are small, we shall omit them throughout our work. Neglecting these contributions, treating the radiative corrections to heavy and light quark lines as being dynamically independent of one another, is known in the literature as the *structure function approximation* [81]. Working in this approximation is equivalent to treating radiative corrections to the heavy and light quark lines as if they originated from two independent copies of the QCD sector, with cross-talk between the two only occurring indirectly, via the electroweak sector [82]. Dropping the $\mathcal{O}(\alpha_{\rm s}^2)$ colour suppressed terms simultaneously removes the problem of how to define our process in the presence of interfering s- and t-channel contributions at this order, since the latter have the same physical origins as the former [45]. Hence, in the context of the approximation within which we are working, the t-channel single-top production process is unambiguously defined.[3]

2.2 Nlops t-channel single-top plus jet

NLO accurate parton shower simulations of s- and t-channel single-top production processes have been constructed in recent years according to the Powheg method, and they have been well used by the ATLAS and CMS collaborations [52]. Our first goal in this work has been to develop a new Nlops simulation of t-channel single-top plus jet production using the Powheg Box framework.

To this end we have obtained the relevant Born and real matrix elements using the MadGraph4-Powheg Box interface presented in ref. [83]. In doing so we omit diagrams with s-channel W bosons that the interface produces by default. The latter restriction was implemented by delicate modifications to the MadGraph4 output. Although all of the correct diagrams are generated by the interface, some of the colour factors associated with subleading-colour contributions in the real-emission matrix elements required manual adjustments. The Powheg Box Born and real matrix elements were subsequently found to yield complete point-by-point agreement with the analogous predictions of Mad-Graph5_aMC@NLO. To remove the interference between the corrections to the light and heavy quark lines and be consistent with the structure function approximation (section 2.1), a semi-automatic script was developed to update the colour matrices present in the real-emission and colour-correlated Born matrix elements. The convergence of the real-emission matrix elements towards the subtraction terms for phase-space points nearing to the soft and/or collinear limits yields a powerful check of the consistency of not only this script, but also the complete implementation of the Born and real matrix elements.

The virtual matrix elements for our Nlops t-channel single-top plus jet simulation have been obtained using the standalone version of MadLoop [74, 84]. The latter was used to generate a library which we have directly linked to our Powheg Box simulation code. The library contains the virtual matrix elements and their associated integral reduction packages, CutTools [75, 76] and IREGI [77], as well as OneLOop [78] for the evaluation of the one-loop scalar integrals. By employing a MadGraph5_aMC@NLO model which

---

[3]This is true to all orders in QCD, yet it fails when higher orders in the weak coupling are considered.

only accounts for NLO QCD corrections, the propagators entering all of our one-loop matrix elements only contain QCD charged particles: the W-boson cannot be part of the loop itself. Thus, the virtual corrections we have generated are fully consistent with the structure function approximation that we have based our work on (see section 2.1).

We have carefully validated our implementation of all of the above elements in the POWHEG BOX, by comparing our predictions for the total NLO cross section, as well as key differential distributions, at fixed order, to those of MADGRAPH5_AMC@NLO. In all cases we found complete agreement between the two codes.

While we do not consider the decays of the top quarks in this work, spin correlations between the top production and decay processes can be important [85]. The latter can be accounted for a posteriori by decaying the top quarks with the MADSPIN program [86, 87]. MADSPIN can parse the Les Houches event files generated by our POWHEG BOX code, simulating the decay of the top quark in each event, including all tree-level correlations between production and decay, to yield a new Les Houches event file wherein all tops have been decayed.

2.3 MINLO

In the POWHEG framework all events generated in the calculation of the NLO cross section have a common associated underlying Born configuration, $\Phi_{\text{STJ}} = \{q_i\}$, with $\{q_i\}$ being the corresponding set of five momenta. The first step in the MINLO procedure is to input the Φ_{STJ} configuration to the exclusive k_t algorithm[4] [80], yielding a $bq \to tq'$ state together with an associated k_t-clustering scale, $\sqrt{y_{12}}$. Denoting the clustering operation $\mathbb{P}$, we notate the resulting set of $2 \to 2$ momenta as $\Phi = \Phi_{\text{ST}} = \{p_i\} \equiv \mathbb{P}[\Phi_{\text{STJ}}]$.

In the limit that $\sqrt{y_{12}}$ is small relative to any hard scales in Φ, the t-channel single-top plus jet cross section is dominated by large Sudakov logarithms at all orders in perturbation theory, rendering fixed order predictions of little or no use, depending on the extent to which the second jet is unresolved. MINLO augments the latter NLO cross section to maintain predictivity when such regions of phase space are probed, by matching it to an all orders summation of these large logarithms, according to the following formula:

$$d\sigma_{\mathcal{M}} = \Delta(y_{12}) \left[d\sigma_{\text{NLO}}^{\text{STJ}} - \Delta(y_{12})|_{\bar{\alpha}_{\text{S}}} \, d\sigma_{\text{LO}}^{\text{STJ}} \right] . \tag{2.1}$$

In eq. (2.1) $d\sigma_{\text{LO}}^{\text{STJ}}$, $d\sigma_{\text{NLO}}^{\text{STJ}}$, and $d\sigma_{\mathcal{M}}$ are the LO, NLO, and MINLO cross sections, fully differential in the three-particle phase space of the single-top plus jet Born-like terms, and the four-particle phase space of their real emission counterparts. All instances of the renormalization and factorization scales in $\Delta(y_{12})$, $d\sigma_{\text{LO}}^{\text{STJ}}$ and $d\sigma_{\text{NLO}}^{\text{STJ}}$ have been set to $\sqrt{y_{12}}$. The MINLO Sudakov form factor is denoted by $\Delta(y_{12})$, with $\Delta(y_{12})|_{\bar{\alpha}_{\text{S}}}$ representing the $\mathcal{O}(\bar{\alpha}_{\text{S}})$ term in its expansion, $\bar{\alpha}_{\text{S}}$ being defined as

$$\bar{\alpha}_{\text{S}} = \frac{\alpha_{\text{S}}}{2\pi} . \tag{2.2}$$

---

[4]Since we aim to provide a fully exclusive simulation and we have access to all particle flavours, we employ a slightly modified version of the exclusive k_t algorithm where we veto clusterings of two particles that cannot be produced by a QCD branching. This is simply achieved by setting the k_t algorithm distance measure to infinity if any two partons that it attempts to combine cannot be associated with the QCD branching of a quark or gluon [63].

The Sudakov form factor can be written as the product of those associated with the light-quark (qq') and the heavy quark (bt) colour dipoles in the leading order single-top process,[5]

$$\Delta(y_{12}) = \Delta_{qq'}(y_{12})\,\Delta_{bt}(y_{12})\,. \tag{2.3}$$

The qq' Sudakov form factor is given by

$$\ln \Delta_{qq'}(y_{12}) \,=\, -2 \int_{y_{12}}^{Q^2_{qq'}} \frac{dq^2}{q^2}\,\bar{\alpha}_{\mathrm{S}}^{\mathrm{CMW}}\,C_F\,\left[\ln \frac{Q^2_{qq'}}{q^2} - \frac{3}{2}\right]\,, \qquad Q^2_{qq'} = 2p_q.p_{q'}\,, \tag{2.4}$$

while the bt Sudakov form factor carries additional terms in the integrand which vanish in the limit $m_t \to 0$,

$$\begin{aligned}
\ln \Delta_{bt}(y_{12}) \,=\, & -2 \int_{y_{12}}^{Q^2_{bt}} \frac{dq^2}{q^2}\,\bar{\alpha}_{\mathrm{S}}^{\mathrm{CMW}}\,C_F\,\left[\ln \frac{Q^2_{bt}}{q^2} - \frac{3}{2}\right] \\
& - \int_{y_{12}}^{Q^2_{bt}} \frac{dq^2}{q^2}\,\bar{\alpha}_{\mathrm{S}}^{\mathrm{CMW}}\,C_F\,\left[\frac{1}{2} - \frac{q}{m_t}\arctan\frac{m_t}{q} - \frac{2m_t^2 - q^2}{2m_t^2}\ln\frac{m_t^2 + q^2}{q^2}\right]\,, \tag{2.5}
\end{aligned}$$

with

$$Q^2_{bt} \,=\, 2p_b.p_t\,. \tag{2.6}$$

The strong coupling is evaluated in the Bremsstrahlung (CMW) scheme [88] with q as its argument in eqs. (2.4)–(2.5):

$$\bar{\alpha}_{\mathrm{S}}^{\mathrm{CMW}} = \bar{\alpha}_{\mathrm{S}}\,[1 + \bar{\alpha}_{\mathrm{S}}K]\,, \qquad K \,=\, \left[\frac{67}{18} - \frac{\pi^2}{6}\right]C_A - \frac{10}{9}\,n_f T_R\,. \tag{2.7}$$

We must stress that our use of $\bar{\alpha}_{\mathrm{S}}^{\mathrm{CMW}}$ here is superfluous in the context of our work, since we do not claim to fully control terms at that order in the Sudakov form factor anyway (NNLL_σ). We note its use merely to accurately document the implementation. For all of the following discussions its presence is irrelevant.[6]

While the $m_t \to 0$ limit of the Sudakov form factor here follows directly from the CAE-SAR formalism[7] [89], we have assembled the form factor with the full top mass dependence using the resummation framework of ref. [90], elaborated on in ref. [91]. We further derived $\Delta_{qq'}$ and Δ_{bt}, independently, by an explicit $\mathcal{O}(\alpha_{\mathrm{S}})$ calculation of the y_{12} distribution using approximations for the matrix elements valid in the soft and quasi-collinear limits. The Sudakov for the light-quark dipole in eq. (2.4) is, as expected, the same as that used in ref. [63], as is the $m_t \to 0$ limit of the bt Sudakov form factor in eq. (2.5). It is easy to see that for $m_t^2 \gg q^2$, there is no double-log term associated to the top quark in Δ_{bt}. Finally, we note that the component of the massive Sudakov form factor owing to quasi-collinear radiation from the top-quark is in agreement with that found in the resummed k_t-jet rate predictions of ref. [92].

---

[5]QCD corrections to the bt and qq' fermion lines in the single-top process are completely independent of one another. Potential contributions to the cross section due to interference of gluons emitted from the two different fermion lines are readily found to be proportional to traces of single Gell-Mann matrices.

[6]Our final numerical results actually suggest that the basic STJ simulation would, by itself, better reproduce NLO inclusive t-channel single-top production predictions, were it to have less of the additional Sudakov suppression that the CMW scheme brings.

[7]With due care to include the soft-wide-angle term for colour dipoles prescribed by that framework (S_1).

2.4 Tuning the Minlo Sudakov form factor

Due to the overall Sudakov form factor in the expression for the cross section, eq. (2.1), our STJ predictions do not diverge in those regions of phase space where the second light parton in the final state (at Born level) becomes unresolved, but instead exhibit a smooth physical Sudakov suppression there. Being finite and physical all through phase space the STJ computation therefore also yields physical predictions for inclusive ST production, where conventional fixed order STJ calculations would instead diverge.

In this subsection we state the accuracy of our STJ simulation for inclusive ST observables, explaining how we have sought to improve on it, while keeping the NLO accuracy for STJ quantities intact. We refer to the improved STJ simulation as STJ*. Since the underlying idea at work here is, at some level, rather simple, the presentation here is kept brief. Expanded explanations of some of the stated results here can be found in appendix A. The results of section 3 can also be somewhat helpful/illustrative in this respect.

To understand the accuracy of the STJ simulation for ST observables, we have studied and clarified the correspondence between its cross section, eq. (2.1), and a NLO-matched resummation formula, accurate at next-to-leading log (NLL_σ) in the perturbative expansion of the cross section[8] (see appendices A.1–A.2). We determine that the source of differences between the two starts, expectedly, at the level of NNLL_σ terms. On integration over y_{12} these NNLL_σ differences give rise to a distribution of Born kinematics different to that of conventional NLO ST by terms of order

$$\int_0^{Q^2} dy_{12}\, \Delta(y_{12})\, \frac{d\sigma_{\mathrm{LO}}^{\mathrm{ST}}}{d\Phi}\, \bar\alpha_{\mathrm{S}}^n\, \frac{1}{y_{12}} \ln^m \frac{Q^2}{y_{12}} \;=\; \frac{d\sigma_{\mathrm{LO}}^{\mathrm{ST}}}{d\Phi} \cdot \mathcal{O}\!\left(\bar\alpha_{\mathrm{S}}^{\,n-\frac{m+1}{2}}\right), \qquad (2.8)$$

with $n \geq 2$ and $m = 2n - 3$ in the case of NNLL_σ terms. In other words, the Minlo-improved STJ simulation has only LO accuracy for ST observables, a fact well supported by our numerical studies in section 3.

Given that the STJ formula, eq. (2.1), already contains, through factorization at the one-loop level, the process-dependent virtual corrections to ST production, we postulate that the only modification needed to promote it to NNLL_σ accuracy is the extension of the Sudakov form factor to that order.[9] If such an extension were then to be implemented in the STJ simulation its y_{12} distribution would converge on that of the NNLL_σ resummation, at the same time eliminating those terms which caused the distribution of its inclusive Born kinematics to deviate from NLO by a relative $\mathcal{O}(\bar\alpha_{\mathrm{S}})$ amount (eq. (2.8)). Residual $\mathrm{N}^3\mathrm{LL}_\sigma$ differences ($m = 2n - 4$) will instead mean that the latter deviations reduce to relative $\mathcal{O}(\bar\alpha_{\mathrm{S}}^{3/2})$. This point is elaborated on in appendix A.3.

We note that it is possible, in principle, to adjust the coefficient of the $\bar\alpha_{\mathrm{S}}^2 \ln^2(Q^2/y_{12})$ term in the Sudakov form factor by a formally subleading y_{12}-independent factor, $\sim 1 + \mathcal{O}(\sqrt{\bar\alpha_{\mathrm{S}}})$, such that the distribution of the ST Born kinematics returned by the STJ calculation (Φ) becomes identical to $d\sigma_{\mathrm{NLO}}^{\mathrm{ST}}/d\Phi$. We further note that the latter form of

---

[8]NLL_σ resummation includes all terms of the form $\frac{1}{y_{12}} \bar\alpha_{\mathrm{S}}^n \ln^m \frac{Q}{y_{12}}$, with $m = 2n - 1$ and $m = 2n - 2$. NNLL_σ resummation further includes all terms with $m = 2n - 3$.

[9]As has been the case for all Minlo simulations that have been proven to reach NLO accuracy for the associated lower multiplicity process so far [69, 79, 93, 94].

the suggested NNLL_σ Sudakov form factor extension is precisely what one would obtain by fitting the $\mathcal{O}(1)$ function $\mathcal{A}_2(\Phi)$ inside

$$\ln \delta \Delta(y_{12}) = -2 \int_{y_{12}}^{Q_{bt}^2} \frac{dq^2}{q^2} \, \bar{\alpha}_{\mathrm{S}}^2 \, \mathcal{A}_2(\Phi) \, \ln \frac{Q_{bt}^2}{q^2} \,, \tag{2.9}$$

such that

$$\frac{d\sigma_{\mathrm{NLO}}^{\mathrm{ST}}}{d\Phi} = \int dy_{12} \, \frac{d\sigma_{\mathcal{M}}}{d\Phi dy_{12}} \, \delta \Delta(y_{12}) \,. \tag{2.10}$$

We have chosen to normalise $\ln \delta \Delta(y_{12})$ with the factor of two on the right-hand side of eq. (2.9), to account for the fact that t-channel single-top production consists of two emitting quark dipoles at lowest order, to enable a more easy/meaningful comparison with other typical Sudakov coefficients at the same order.

Eq. (2.10) summarises the improvement procedure which we have applied to our baseline STJ construction described in sections 2.2–2.3. The fit procedure to arrive at $\mathcal{A}_2(\Phi)$ in eq. (2.9) can be attempted in a variety of ways, and we have chosen to use an advanced procedure based on neural network techniques, for which we give details in section 2.5. In practice, we have implemented the Sudakov form factor correction, $\delta \Delta(y_{12})$, evaluating the q^2 integral in eq. (2.9) with a one-loop running coupling:

$$\ln \delta \Delta(y_{12}) = \mathcal{A}_2(\Phi) \, \mathcal{G}_2(\lambda) \,, \qquad \mathcal{G}_2(\lambda) = \frac{-1}{2\pi^2 \beta_0^2} \left[\frac{2\lambda + (1-2\lambda)\ln(1-2\lambda)}{1-2\lambda} \right] \,, \tag{2.11}$$

with

$$\beta_0 = \frac{11 C_A - 2 n_f}{12\pi} \,, \qquad \lambda = \frac{1}{2} \alpha_{\mathrm{S}} \beta_0 \ln \frac{Q_{bt}^2}{y_{12}} \,. \tag{2.12}$$

While we use a form for the y_{12} resummation formula at NNLL_σ, we do not presume to know the details of the related Sudakov ingredients at that order, so we assume that the $\mathcal{A}_2$ coefficient has a general dependence on Φ already for this reason. There are, however, established grounds to expect $\mathcal{A}_2$ to be generically Φ-dependent, as also elaborated in appendix A.3.

We also point out that, if it is the case that the differences between the STJ and NLO ST Φ-distributions owe purely to the omission of terms in the Sudakov form factor, the $\mathcal{A}_2$ function fitted in this work, for a given 13 TeV LHC setup, should remain valid for different beam energies, PDF sets, etc. We have carried out empirical investigations regarding this point, using the STJ* Minlo Sudakov form factor fitted using samples of ST and STJ generated for a 13 TeV LHC, to make predictions at 8 TeV. We find that the STJ* simulation with the latter fit reproduces inclusive 8 TeV t-channel single-top observables remarkably well. A representative sample of results from that study is given in appendix B. Indeed, the latter results strongly suggest that a dedicated refitting of the STJ* Sudakov form factor, using 8 TeV ST and STJ events, would fare comparably to the one based on fitting with 13 TeV events.

Should the missing NNLL_σ terms in the Minlo Sudakov form factor of STJ not fully account for the leading ($\mathcal{O}(\bar{\alpha}_{\mathrm{S}})$) deviations in its Φ distribution with respect to NLO ST predictions, the modification in eq. (2.10) is still admissible, provided that the fitted $\mathcal{A}_2$

is of the same order of magnitude as other Sudakov coefficients. It does not compromise the NLO accuracy of the STJ generator for t-channel single-top plus jet observables, or change its resummation accuracy.

Finally, it is reasonable to ask why we have chosen to use Q_{bt} for the hard scale in eq. (2.9) rather than $Q_{qq'}$. Without a much more sophisticated NLO calculational framework, wherein one has the ability to clearly distinguish which contributions to the NLO cross section are associated to which colour dipole in the leading order process (qq'/bt), it is not possible to carry out the correction procedure proposed here on a dipole-by-dipole basis. Hence, we are limited to having one cross section unitarity constraint which we can use to fit one term in Sudakov form factor. This does not pose a great problem in practice, since regions of the ST Born phase space where Q_{bt} can be disparate from $Q_{qq'}$ are strongly suppressed. Moreover, in the context of the STJ generator, the great bulk of events populating such regions are always anyhow subject to large Sudakov logarithms associated with soft corrections to the bt system. We have assessed ambiguities related to choosing Q_{bt} as the hard scale in $\delta\Delta(y_{12})$ conservatively (varying Q_{tb} up and down by a factor of four), finding a negligible impact in all of the $\mathcal{O}(200)$ distributions considered in our studies. These uncertainties are depicted in *all* of the plots of our results section, 3, as dark red bands, but for the most part they are so small as to be invisible.

2.5 Neural network fit

In this section we describe how we have fitted the $\mathcal{A}_2(\Phi)$ Sudakov coefficient in eqs. (2.9)–(2.11), through imposing the differential unitarity constraint expressed in eq. (2.10). With the fitted $\mathcal{A}_2(\Phi)$ in hand we then simply reweight STJ→STJ* events by multiplying them with the Sudakov form factor correction, $\delta\Delta(y_{12})$, as in the integrand on the right-hand side of eq. (2.10).

To quicken the development of the method and give it much greater flexibility, in implementing our tuning procedure for the MINLO Sudakov form factor, we have chosen to define the Born variables, Φ, slightly differently to how they were introduced at the beginning of section 2.3. For the purposes of this part of the work, they are defined from the set of momenta that result from applying the exclusive k_t algorithm to the events in the Les Houches files output by the ST and STJ generators; rather than from directly clustering the underlying Born configurations in the case of the STJ simulation. It is natural to expect that differences resulting from this modification are small, since the effective clustering represented by the inverse of the POWHEG BOX FKS mapping [91, 95] is based on the transverse momentum separation of partons in the soft and collinear limits, as in the k_t algorithm. This is nevertheless an approximation, made of convenience rather than necessity. However, as noted at the end of section 2.4, and as we shall go on to demonstrate in section 3, the MINLO tuning procedure we have carried out is remarkably robust even against strong variations in its associated parameters, e.g. the hard scale in $\delta\Delta(y_{12})$, eq. (2.9).

Being a $2 \to 2$ scattering process at leading order, the Born phase space of t-channel single-top production can be parametrized using three independent variables. There is freedom in the selection of these variables, and we have opted for simple quantities which

are rather uncorrelated from one another. As stated above, the Born variables are defined from the two momenta associated with the final-state after clustering the events in the ST and STJ Les Houches files with the exclusive k_t algorithm, until each one consists of just the top quark and a light jet, whose momenta we label p_t and p_j.[10] From the latter we construct our chosen Born variables: y_{tj}, the rapidity of $p_t + p_j$; $\hat{y}_t$, the rapidity interval between the top quark and the latter; and $p_{t,\text{top}}$, the transverse momentum of the top.

Since the constraint to be solved for $\mathcal{A}_2(\Phi)$, eq. (2.10), involves a *convolution* of the STJ cross section with $\delta\Delta(y_{12})$, eq. (2.11), we discretize the three dimensional space spanned by the Born variables, in order to use eq. (2.10) to fit $\mathcal{A}_2(\Phi)$ using samples of ST and STJ Les Houches events.[11] The discretization is carried out by first creating a regular binning in the physically accessible region of the $\hat{y}_t - y_{tj}$ plane, wherein each bin covers 0.5×0.5 units of rapidity. Each of the latter 2D bins is further segmented according to $p_{t,\text{top}}$, in such a way that all resulting bins in the three dimensional parameter space contain 2000 of the 18 million STJ events used in carrying out the subsequent fit.[12]

The fitted $\mathcal{A}_2(\Phi)$ function is then determined by minimizing the following loss function:

$$\mathcal{L} \;=\; \sum_{i=1}^{N_{\text{bins}}} \left[\sum_{j=1}^{N} w_{i,j}^{\text{ST}} - \sum_{k=1}^{N'} w_{i,k}^{\text{STJ}} \, e^{\tilde{\mathcal{A}}_2(\Phi_i)\,\mathcal{G}_2(\lambda)} \right]^2 . \tag{2.13}$$

Here, in eq. (2.13), N_{bins} is the total number of bins in the discretized three dimensional Born variable parameter space. N and N' are, respectively, the number of ST and STJ events used in carrying out the fit. $w_{i,j}^{\text{ST}}$ is the weight of the jth ST event in bin i of the discretized Born variable parameter space, with $w_{i,k}^{\text{STJ}}$ being analogously defined for the STJ events. $\tilde{\mathcal{A}}_2(\Phi)$ in eq. (2.13) is the model prediction for the desired effective Sudakov form factor coefficient (eqs. (2.9)–(2.11)), evaluated at the centre of bin i. $\mathcal{G}_2(\lambda)$ is as defined in eq. (2.11).

The fit of $\mathcal{A}_2(\Phi)$ according to eq. (2.13) is performed with machine learning techniques. To avoid making assumptions regarding the analytic form of $\mathcal{A}_2(\Phi)$, we have employed an artificial neural network parametrization based on a feed-forward multi-layer perceptron. This choice eliminates the requirement of selecting a specific functional form for our problem, by providing a non-linear model which learns the data structure. Additionally, the $\mathcal{A}_2(\Phi)$ function fitted in this way evaluates quickly when called on to reweight STJ→STJ* events with the Sudakov form factor correction, $\delta\Delta(y_{12})$.

A grid search was carried out to determine the best neural network architecture, loss function definition, and optimizer algorithm for our framework. The best architecture was found to consist of a neural network with two hidden layers, comprising five and three

---

[10]Rarely an event will fail to cluster back to a two-body ST final-state, due to the flavour conservation implemented in our k_t clustering (footnote 4). Having no associated ST Born configuration, such events are omitted from the $\mathcal{A}_2(\Phi)$ fitting procedure, and are untouched by the related reweighting.

[11]An alternative reweighting method, based on weighted kernel density estimation, has been explored as well. In this method the discretization of the phase-space can be avoided, but it comes with a huge computational cost and large memory usage and has therefore been disregared.

[12]At the edges of the phase space adjacent bins are combined, iteratively, if they are found to contain less than 2000 events.

nodes respectively, based on hyperbolic tangent activation functions.[13] The output layer for the architecture consists of a single node with a linear activation function. In total this model requires the tune of 42 parameters in the form of weights and biases. An efficient genetic optimizer was implemented to train the model, based on the covariance matrix evolution strategy (CMA-ES) [96].

Fits to the $\mathcal{A}_2(\Phi)$ function were carried out with the latter neural network setup, using samples of 25 million ST and 18 million STJ POWHEG Les Houches events, at a 13 TeV LHC.[14] The same setup and statistics were also used to perform analogous fits for the case of single-anti-top production. Both for t-channel single-top and single-anti-top processes eleven $\mathcal{A}_2(\Phi)$ fits were carried out. Seven of these correspond to redoing the fit in the presence of correlated renormalization and factorization scale variations in the ST and STJ generators; i.e. we perform a separate fit of $\mathcal{A}_2(\Phi)$ varying $\mu_{R/F} \to K_{R/F}\,\mu_{R/F}$, in both the ST and STJ simulations, for all pairings of K_R and K_F values in $\{\frac{1}{2}, 1, 2\}$, discarding the two pairings where K_R and K_F differ by more than a factor of two. For the central scale choice, four further $\mathcal{A}_2(\Phi)$ fits are carried out for which the scale Q_{bt} in $\delta\Delta(y_{12})$, eq. (2.9), is multiplied by $K_{Q_{bt}} \in \{\frac{1}{4}, \frac{1}{2}, 2, 4\}$, in order to gauge sensitivity to that scale choice.

In figure 1 we project the trained neural network model obtained with the setup described in section 3.1, for the central renormalization and factorization scale choice in t-channel single-top production, into the $\hat{y}_t - p_{t,\text{top}}$ plane, for $y_{tj} = 0.0$ (left plot), $y_{tj} = 1.5$ (centre plot), and $y_{tj} = 3.0$ (right plot). To gain some perspective on the size of the $\mathcal{A}_2$ values shown in the heatmap plots of figure 1, we point out that the function multiplying it in the Sudakov form factor in our work, $\mathcal{G}_2(\lambda)$, eq. (2.11), is precisely the same as that multiplying the A_2 coefficient in eq. (10b) of ref. [97]; modulo an extra factor of two in our case, accounting for the fact that we have two colour dipoles in our lowest order process, while those considered in ref. [97] consist of just one. In ref. [97] $A_2 \simeq 9$ for the Drell-Yan process, and $A_2 \simeq 21$ in the case of Higgs production via gluon fusion. We conclude that the fitted $\mathcal{A}_2(\Phi)$ is numerically of similar size to these A_2 coefficients in the entire phase space.

3 Results

In the following we discuss a representative sample of distributions obtained in the context of our validation of the new STJ NLOPS generator, as set out in sections 2.1–2.3, along with its improved STJ* counterpart, based on the fitting of the Sudakov form factor described in sections 2.4–2.5. We remind that both STJ and STJ* simulations aim at NLO accuracy in the description of t-channel single-top plus jet events, while the latter is also intended to be NLO accurate in the description of generic inclusive t-channel single-top observables. The POWHEG NLOPS simulation of t-channel single-top production, ST [52], is used throughout

---

[13]In the grid search procedure several models and training setups are tested and the setup which obtains the lowest cost function is proposed as the best model.

[14]Details on the values of physical constants and other parameters used to generate these samples follow at the beginning of section 3.
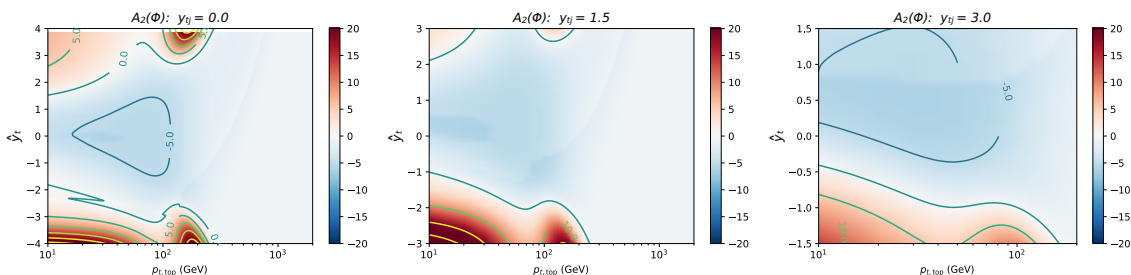
Figure 1. Heatmap plots of the fitted $\mathcal{A}_2(\Phi)$ term in the MINLO Sudakov form factor, defined through eqs. (2.9-2.11); used in promoting STJ→STJ* events by reweighting the former with the NNLL$_\sigma$ exponential factor, $\delta\Delta(y_{12})$ (eq. (2.11)). The $\mathcal{A}_2(\Phi)$ shown here has been obtained using the default (central) scale choices in the ST and STJ generators, for $y_{tj} = 0.0$ (left plot), $y_{tj} = 1.5$ (centre plot) and $y_{tj} = 3.0$ (right plot). The ranges in each of the three plots vary in order to limit the amount of physically inaccessible phase space shown, while not cutting away any accessible regions.

to assess the quality of the description afforded by STJ and STJ* for inclusive quantities, and to gauge the magnitude of NLO effects in t-channel single-top plus jet events.

3.1 Setup

Both here in our validation studies and in fitting the MINLO Sudakov form factor, we have considered 13 TeV LHC collisions. We use the NNLO NNPDF 3.0 parton distribution functions [98] corresponding to $\alpha_{\mathrm{s}}(m_Z) = 0.118$ via the LHAPDF package [99] (index 261000). The Fermi constant is set to $G_F = 1.16639 \times 10^{-5}\,\mathrm{GeV}^{-2}$. The Z-boson mass is set to $m_Z = 91.118\,\mathrm{GeV}$, and the fine structure constant evaluated at that scale is given by $1/\alpha = 127.012$. The W-boson mass, the weak mixing angle, and the weak coupling constant are hence derived according to tree-level relations among the electroweak parameters. The top quark mass has been set to $172.5\,\mathrm{GeV}$, while all other quark masses have been set to zero.

We use a diagonal CKM matrix. On the heavy quark line, where the bottom quark converts to a top quark, we therefore have $V_{tb} = 1$, which is well within the uncertainties on its current determination from Tevatron and LHC data $|V_{tb}| = 1.009 \pm 0.031$ [100]. If we further sum over the flavours of the final-state quark on the associated light quark line, since the CKM matrix is unitarity, our matrix elements will be identical to those obtained with the full CKM matrix.

All results shown in this section include the effects of parton showering, simulated with the PYTHIA8 program [101]. Since our primary intention is to validate the new STJ generator and its tuned STJ* counterpart, we have switched off hadronization and multiple parton interactions in PYTHIA8, and we treat the top quark as a stable particle.[15] We have found it important to adopt a new momentum reshuffling option in PYTHIA8,[16] intended

---

[15]We remind that one can relatively quickly produce new Les Houches event files in which the top quarks have been decayed, according to the relevant tree-level matrix elements, using MADSPIN [86, 87].

[16]We set `SpaceShower:dipoleRecoil = on` in the PYTHIA8 input file. Ref. [102] describes in detail the physical reasoning behind this option and how it modifies the showering of initial-final QCD dipoles. It

to yield an alternative treatment of showering initial-final QCD dipoles [102]. Similar findings in recent studies on vector boson scattering simulations have been commented on in ref. [103].

In the ST simulation the central renormalization and factorization scale choice is $\mu_R = \mu_F = m_t$. Theoretical uncertainties are estimated by varying μ_R and μ_F, independently, up and down by a factor of two, while keeping $\frac{1}{2} \leq \mu_R/\mu_F \leq 2$. The envelope of the predictions following from these variations defines the theoretical uncertainty. For STJ the central scale choice is dictated by the MINLO prescription in section 2.3, with uncertainties being estimated in complete analogy to the ST case. The theoretical uncertainties for STJ* follow as in the STJ case, but with $\mathcal{A}_2(\Phi)$ changing according to μ_R and μ_F, to maintain the equality in eq. (2.10), with μ_R and μ_F being varied about their central values in the same way on both sides of that equation.

As mentioned at the end of sections 2.4 and 2.5, we also investigate the uncertainty in STJ* predictions owing to the ambiguity in choosing Q_{bt} as the hard scale in the NNLL$_\sigma$ reweighting factor $\delta\Delta(y_{12})$ (eq. (2.9)). This uncertainty is estimated by taking the envelope of predictions obtained by rescaling Q_{bt} in $\delta\Delta(y_{12})$ up and down by a factor of four, fitting a new $\mathcal{A}_2(\Phi)$ for each Q_{bt} variation, so as to maintain eq. (2.10). This uncertainty is almost always too small to be visible in our results, and never exceeds that due to renormalization and factorization scale variation.

Finally, in validating our simulations, we have studied the same extensive range of distributions obtained from an 8 TeV LHC setup, identical to the 13 TeV one described above. The 8 TeV analysis was carried out without refitting the MINLO Sudakov form factor for STJ*, which remains the same as in the 13 TeV study immediately following below. A representative subset of these 8 TeV predictions is deferred to appendix B, to avoid repetition, since the findings are very much the same as for the 13 TeV case discussed here, in sections 3.3–3.7.

3.2 Guide to plots

All plots in this section show predictions, with uncertainty estimates, from the ST simulation in green, STJ in blue, and the tuned STJ* generator in red. In each case the top panel shows absolute cross section predictions, while the lower three panels display ratios of the various results to one another. Q_{bt} variation in $\delta\Delta(y_{12})$ (eq. (2.9)) is depicted by dark red shading, but is often too small to be visible.

The order of the presentation roughly follows the degree of exclusivity of the studied observables, starting with the most inclusive, for which the ST and STJ* simulations should be NLO accurate, working towards more exclusive quantities, for which STJ and STJ* should provide the best predictions.

3.3 Top quark rapidity and transverse momentum

In figure 2 we present predictions for the top quark rapidity and transverse momentum distributions. Being inclusive with respect to all jet activity, the ST simulation (green)

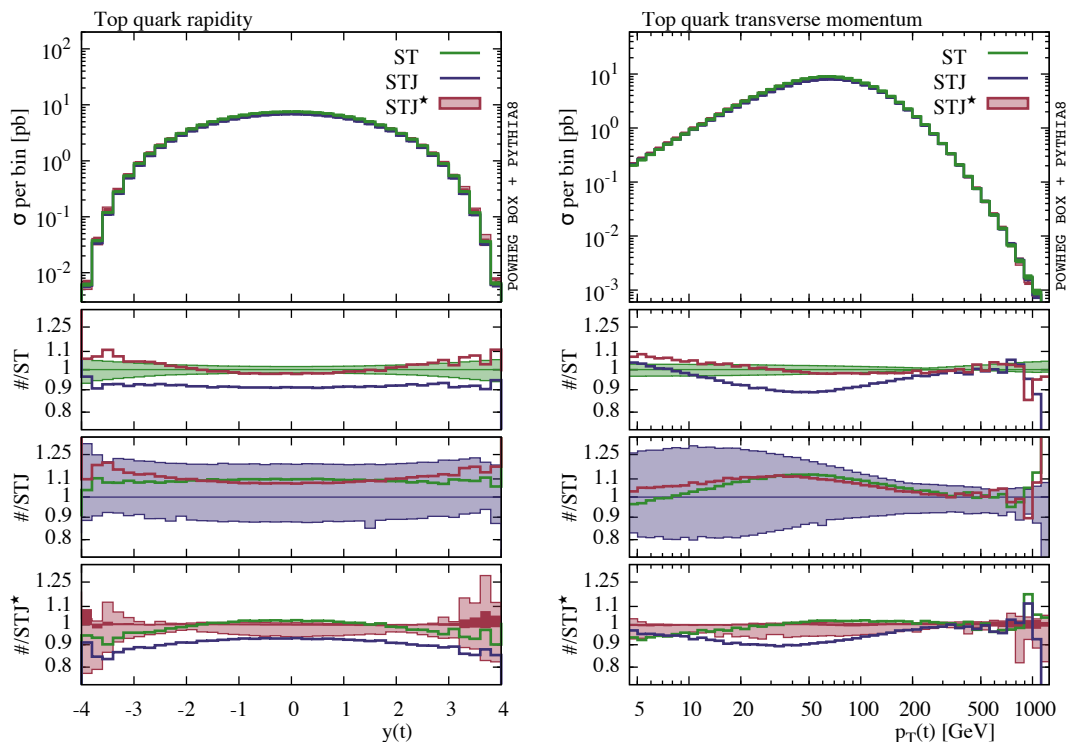states that this option is theoretically better motivated than its alternatives.

Figure 2. Rapidity (left) and transverse momentum (right) of the top quark in t-channel single-top production. Predictions from the POWHEG ST program [52] are shown in green. Results from the new MINLO STJ simulation are displayed in blue, while those of its improved counterpart, STJ*, appear in red. All predictions include parton shower effects simulated by PYTHIA8 [101].

provides NLO accurate predictions for these observables, while STJ (blue) is formally only LO accurate (section 2.4 and appendix A.2). This statement is substantiated by the two distributions in figure 2. The inclusive ST predictions carry a remarkably small QCD scale uncertainty at NLO, as is well known to be the case for inclusive t-channel single-top observables, with the STJ predictions lying no more than 10% away from the latter, throughout almost all of the two distributions, and with a larger associated uncertainty, compatible with the fact that it is only LO accurate.

In the case of the top quark rapidity distribution the improved STJ* simulation agrees with the ST results to within $\lesssim 2\%$ in the central region, deviating slightly from it, by $\sim 6\%$, at high values of the absolute rapidity, $|y(t)| > 3$. These deviations are, nevertheless, just of the same size as the ST scale uncertainties in these regions, modulo some statistical fluctuations.

Besides the central prediction of STJ* converging on that of the ST simulation, so too does its scale uncertainty band. The uncertainty band of the ST simulation is as small as $\pm 3\%$ in the central $y(t)$ region of the first ratio plot. The STJ* uncertainty band in the third ratio plot is at the level of $+2\%/-6\%$ in the same region, to be compared with $+20\%/-10\%$ in the STJ case.

At the extremities of the top quark rapidity distribution, $|y(t)| \gtrsim 3.5$, the STJ* uncertainty band exceeds that of ST, and looks somewhat more like that of STJ. Such

imperfections are not entirely unexpected in these regions due to limited statistics, especially when working with the weighted events that determine the scale variations, which carry greater statistical noise in the neural network fitting procedure than those determining the central prediction. The discretization of the Born variable parameter space used in the fit can also become coarse in these lowly populated high-rapidity regions. In addition, it is worth remembering that the neural network model makes no assumptions, whatsoever, on the form of the function to be fitted, and is ultimately limited to just 42 parameters.

Further refinement and/or complexity in our STJ* neural network model, could increase the level of convergence of the STJ* uncertainty band to that of ST. However, the improvement in both the description of the central value and the band, from STJ→STJ*, is, nevertheless, highly satisfactory, particularly when considered in the context of earlier works on Minlo' [69, 93, 94].

The top quark transverse momentum distribution, in the right-hand plot of figure 2, shows a similarly expected and pleasing pattern of results. As for $y(t)$, there is a very small scale uncertainty associated to the NLO accurate ST predictions for this observable, not exceeding $\pm 4\%$. The central scale, LO accurate STJ prediction — which is simply divergent without the Minlo prescription of section 2.3 — lies within 10% of the central ST one below $p_{\rm T}(t) = 1\,{\rm TeV}$. Again, the STJ result exhibits a relatively large uncertainty band, consistent with that seen in the $y(t)$ distribution. By contrast, the STJ* prediction sits within $\pm 2\%$ of the NLO accurate ST result all through the range $10 < p_{\rm T}(t) < 1250\,{\rm GeV}$. For $p_{\rm T}(t) < 10\,{\rm GeV}$ the STJ* prediction deviates by up to 7% from the central ST prediction. However, the cross section is falling very steeply in this part of the spectrum, reducing by a factor of ~ 5, in the interval $5 < p_{\rm T}(t) < 10\,{\rm GeV}$.

3.4 Inclusive jet cross sections

Figure 3 shows the inclusive jet cross sections in t-channel single-top production, for jets formed by the radius $R = 1$ k_t algorithm, on the left, and the $R = 0.4$ anti-k_t algorithm, on the right. In both cases a transverse momentum cut of $25\,{\rm GeV}$ is applied in defining the jets. The $R = 1$ inclusive k_t jet cross sections are primarily of technical interest, being the inclusive version of the jet definition used in tuning the STJ Minlo Sudakov form factor. The $R = 0.4$ anti-k_t jet cross sections are more experimentally relevant, since this is the typical jet definition employed in LHC analyses.

For both jet definitions the results shown in figure 3 are very much just as we would like. The $N_{\rm jets} \geq 0$ and $N_{\rm jets} \geq 1$ cross sections are inclusive t-channel single-top production observables, receiving their leading contributions in perturbation theory from the lowest order $bq \to tq'$ process. Accordingly, the ST predictions (green) are NLO accurate in describing these jet bins. Conventional fixed order t-channel single-top plus jet predictions for the same cross sections would be divergent. In contrast, through inclusion of the Minlo procedure (section 2.3), the predictions of the STJ simulation (blue) lie just $\sim 10\%$ below those of the NLO accurate ST results. The central prediction of the STJ* code, with the tuned Minlo Sudakov form factor (red), further improves on the latter, and converges exactly onto the NLO ST predictions in the same two jet bins.
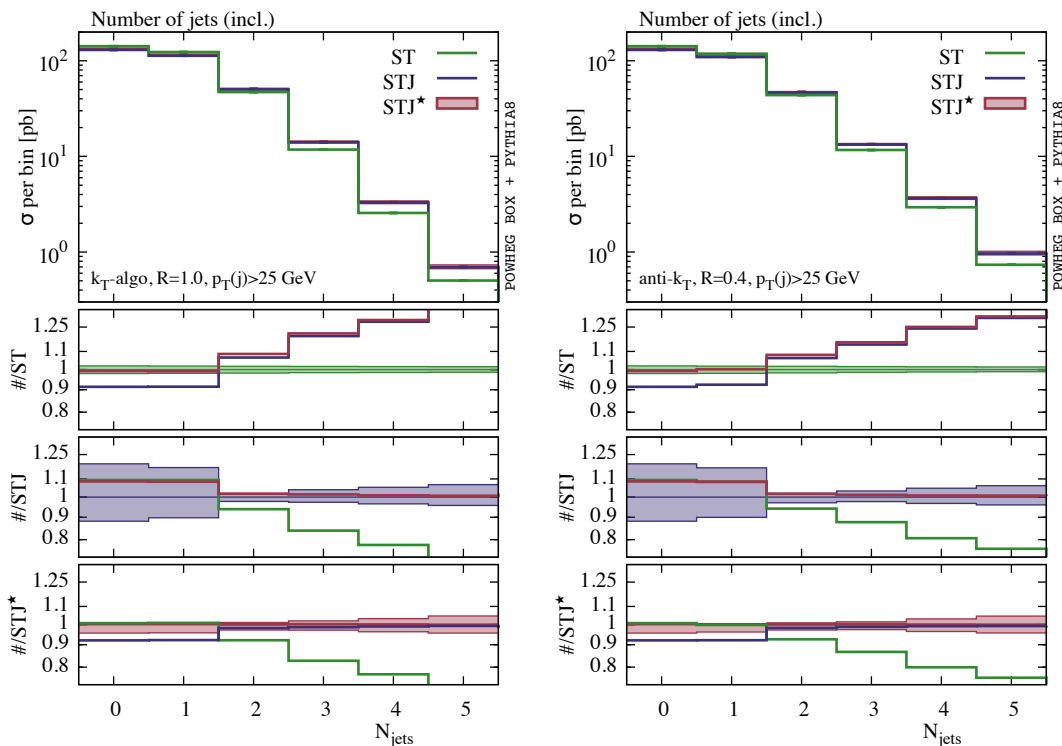
Figure 3. Inclusive jet cross sections in t-channel single-top production, with a jet transverse momentum threshold of $25\,\text{GeV}$. The left-hand plot shows predictions for jets defined according to the k_t clustering algorithm with radius parameter $R = 1$, while the right-hand plot gives the analogous predictions for the case of the anti-k_t algorithm with $R = 0.4$. As in figure 2 we show in green, blue and red, predictions from the ST, STJ and STJ* simulations respectively.

Looking to the higher multiplicity cross sections, for $N_\text{jets} \geq 2$ we see the STJ* generator now exactly aligns with the STJ predictions, as opposed to those of ST. The ST cross sections fall below those of STJ and STJ* by an amount which increases with N_jets. Both the STJ* and STJ predictions in the $N_\text{jets} \geq 2$ and $N_\text{jets} \geq 3$ bins, are NLO and LO accurate respectively. On the other hand, in the ST case, the description of $N_\text{jets} \geq 2$ is LO accurate, while events in the $N_\text{jets} \geq 3$ bin are due entirely to parton showering. The undershooting of jet cross sections by simulations based on lower multiplicity matrix elements, compared to those built from higher multiplicity ones, is a typical observation in comparisons of event generators based on matrix element-parton shower matching/merging.

3.5 Differential jet rates

The $n \to m$ differential jet rates, y_{nm}, measure the value of the distance measure in the exclusive k_t clustering algorithm at which an n-jet event becomes resolved as an m-jet one. They are key variables of interest in validating our STJ and STJ* generators.

The $\sqrt{y_{01}}$ jet rate, on the left-hand side of figure 4, is essentially equivalent to the transverse momentum spectrum of the hardest jet obtained in the inclusive k_t clustering algorithm, with jet radius $R = 1$. Hence $\sqrt{y_{01}}$ is therefore described with NLO accuracy by the ST simulation and LO accuracy by STJ. Correspondingly, except for the region
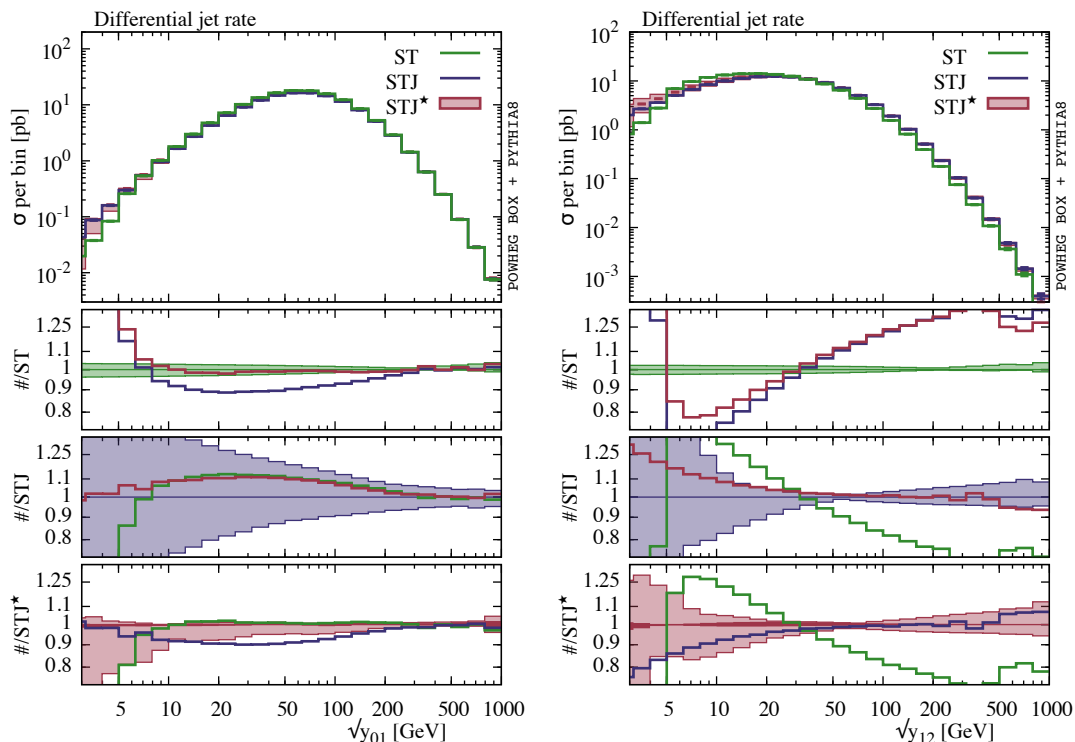
Figure 4. Differential jet rates in the exclusive k_t clustering algorithm [80], with jet radius parameter $R = 1$. The left-hand plot presents predictions for the $0 \to 1$ jet rate, $\sqrt{y_{01}}$, corresponding to the value of the distance measure in that algorithm at which a 1-jet event would become resolved as a 0-jet one. The right-hand plot shows the $1 \to 2$ jet rate, $\sqrt{y_{12}}$, analogously defined. As in figures 2 and 3, all predictions include the effects of parton showering provided by PYTHIA8, and follow the same colour conventions.

$\sqrt{y_{01}} \lesssim 5\,\text{GeV}$, the blue STJ prediction lies within $\sim 10\%$ of the green ST result. In the same region, all the way up to $\sqrt{y_{01}} = 1\,\text{TeV}$ the central STJ* prediction lies within the tiny ST scale uncertainty band, which is never more than $\pm 4\%$ wide. Moreover, the STJ* scale uncertainty band is, again, greatly shrunk with respect to that of the STJ simulation, being at the level of $+2\%/-6\%$ down to $\sqrt{y_{01}} \lesssim 10\,\text{GeV}$. This level of agreement is satisfying considering that a linear plot of the leading jet transverse momentum spectrum (not shown) reveals that the cross section falls by five orders of magnitude in the interval $10 \to 1000\,\text{GeV}$.

As we approach $5\,\text{GeV}$ in the $\sqrt{y_{01}}$ spectrum from above, we observe a sharp irregular behaviour from the NLO accurate ST generator. In particular, the latter distribution exhibits a sharp downward step with respect to the STJ and STJ* predictions. This same trend is also clear very close to $5\,\text{GeV}$ in the transverse momentum spectra of the first and second jets (not shown). The feature arises due to the fact that the ST program generates real radiation events from $bq \to tq'$ underlying Born configurations via the POWHEG Sudakov form factor. The latter Sudakov form factor exponent contains b-quark PDFs in its numerator and denominator, evaluated at the transverse momentum scale of the would-be emitted radiation, $p_{\text{T,rad}}$. The b-quark PDFs evaluate to zero as soon as $p_{\text{T,rad}} < m_{b,0}$,

where $m_{b,0}$ is the value of the factorization scale at which the b-quark density is turned on or off in the relevant PDF set. Finally, we stress that the significance of these irregularities in the differential jet rates and jet transverse momentum spectra should not be overstated, since they occur only at low scales that are of limited phenomenological and experimental relevance.

We now turn our attention to the $\sqrt{y_{12}}$ distribution shown on the right-hand side of figure 4. This distribution is both very important and informative in checking the effects due to the MINLO tuning procedure, since it is precisely this quantity, albeit defined at the level of pre-shower Les Houches events, which the tuning acts on directly. This distribution therefore measures very well the cost, or any potential breakage, associated with promoting STJ→STJ*.

Away from the Sudakov peak region, $\sqrt{y_{12}} \gtrsim 20\,\mathrm{GeV}$, where it is meaningful to talk of accuracy defined in terms of fixed order perturbation theory, the ST simulation is only LO accurate, while STJ is NLO accurate. As expected, we see that the STJ* simulation, which fully aligns with the ST predictions above $10\,\mathrm{GeV}$ in the $\sqrt{y_{01}}$ spectrum, here, instead, agrees with STJ to the right of the Sudakov peak in $\sqrt{y_{12}}$. Below $\sqrt{y_{12}} = 30\,\mathrm{GeV}$ the central STJ and STJ* results begin to slowly deviate from one another, due to the effects of the tuning in the latter's MINLO Sudakov form factor; the differences reach 3-4% at $\sqrt{y_{12}} = 20\,\mathrm{GeV}$, rising to 8% deep in the Sudakov region at $\sqrt{y_{12}} = 10\,\mathrm{GeV}$, with neither prediction ever departing outside the other one's scale uncertainty band. We can see from this plot that the relatively low STJ cross sections observed for inclusive quantities and low multiplicity jet cross sections, in sections 3.3–3.4, are compensated for in the STJ* simulation by the uplift in its $\sqrt{y_{12}}$ spectrum with respect to that of STJ, both on and below the Sudakov peak in the $\sqrt{y_{12}}$ distribution. It is further clear from this spectrum that the NLO accuracy of STJ for t-channel single-top plus jet observables has been fully inherited by the tuned STJ* simulation.

Finally, we remark that the same smallness of the ST uncertainty band seen in the $\sqrt{y_{01}}$ distribution persists in the $\sqrt{y_{12}}$ spectrum and is, again, an underestimate of the true uncertainty. It is an artefact of the POWHEG NLOPS methodology, whereby the scale compensation associated with NLO accurate $bq \to tq'$ underlying Born kinematics is spread out all through the single-top plus jet phase space. The ST uncertainty is also underestimated in the region below the peak at $10\,\mathrm{GeV}$, which is dominated by large Sudakov logarithms at all orders and by non-perturbative effects. The STJ and STJ* simulations are, conversely, NLO rather than LO for this distribution, and while they carry larger uncertainty bands than ST, their estimates should be considered to be much more realistic for the $\sqrt{y_{12}}$ spectrum.

3.6 Top-jet angular correlations

Angular correlations between the top quark and the leading jet are somewhat complementary to the $\sqrt{y_{12}}$ differential jet rate just discussed, since they also probe across the transition between topologies involving one and two resolved jets, albeit now in terms of angles.
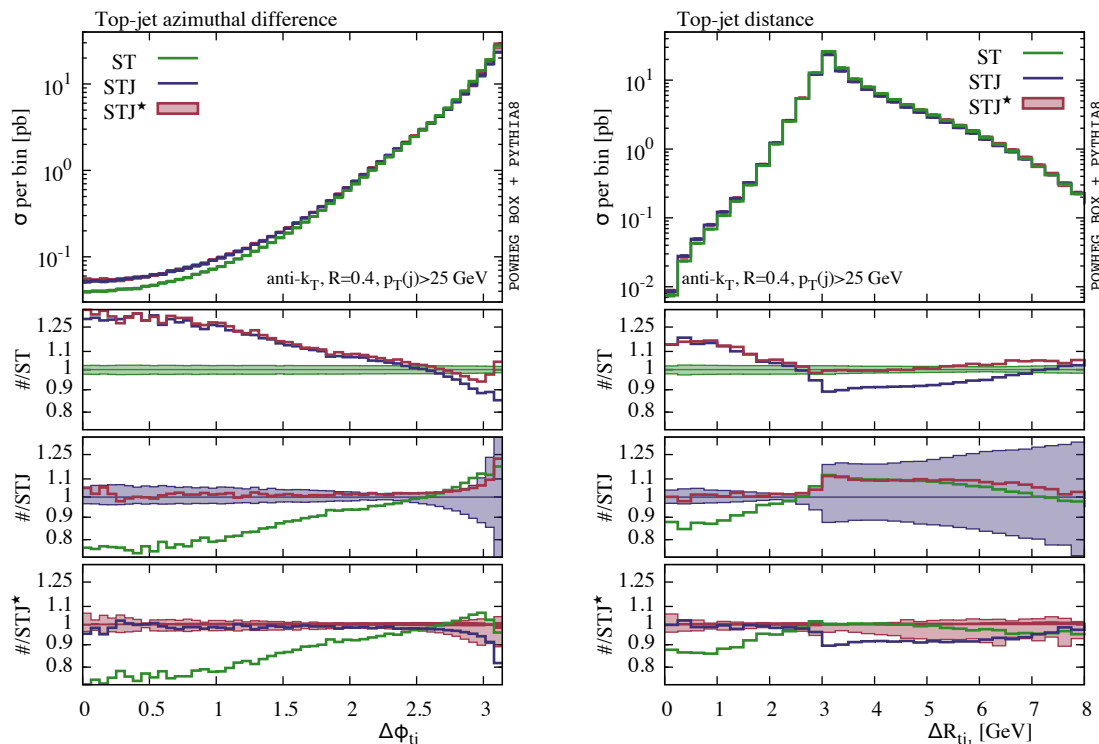
Figure 5. The azimuthal separation of the top quark and the leading jet (left), and the $\eta - \phi$ plane distance, $\Delta R_{tj_1} = (\Delta\phi_{tj}^2 + \Delta\eta_{tj}^2)^{\frac{1}{2}}$, between the same two objects (right). Predictions from the POWHEG ST program [52] are shown in green. Results from the new MINLO STJ simulation are displayed in blue, while those of its improved counterpart, STJ*, appear in red. All predictions include parton shower effects simulated by PYTHIA8 [101].

On the left of figure 5 we show the azimuthal separation between the top quark and the leading jet in t-channel single-top production. At lowest order in perturbation theory this distribution would consist of a lone spike at $\Delta\phi_{tj} = \pi$, since at that order the top quark and the light parton must exactly balance each other's transverse momentum. Additional soft-collinear radiation on top of the latter smears the spike out into the peak seen around $\Delta\phi_{tj} = \pi$, in the left-hand plot of figure 5. Furthermore, the integral of the $\Delta\phi_{tj}$ distribution must, by definition, yield the inclusive 1-jet cross section of figure 3. Thus, the normalizaton of this distribution, which is largely set by the peak region, is described with NLO accuracy by ST and LO accuracy by STJ. Taking the above points together, it then makes sense that we see the STJ* program tend to the ST prediction in the peak region. Indeed, the $\sim 10-15\%$ deficit between the STJ prediction and that of ST, in the region $\Delta\phi_{tj} = \pi$, correlates with the $\sim 10\%$ deficit seen in the inclusive 1-jet cross section on the right of figure 3. Equally, the agreement of ST and STJ* in the peak region is reflective of the corresponding agreement in the inclusive 1-jet cross section of figure 3.

Moving off the peak region in $\Delta\phi_{tj}$, the distribution becomes increasingly populated by topologies involving the top quark recoiling against two jets, or more. In fact the region $\Delta\phi_{tj} \lesssim 2\pi/3$ is not accessible if the top quark only recoils against two final-state objects. Correspondingly, off the peak region, the STJ simulation can be expected to give the most

– 21 –

accurate predictions (NLO). Pleasingly, and expectedly, we see the STJ* simulation is indistinguishable from the STJ prediction already for $\Delta\phi_{tj} \lesssim 2.6$.

The distribution on the right-hand side of figure 5 plots the angular distance between the top quark and the leading jet in the $\eta - \phi$ plane: $\Delta R_{tj} = (\Delta\phi_{tj}^2 + \Delta\eta_{tj}^2)^{1/2}$. The events populating the peak region in this plot are predominantly those in the peak of the $\Delta\phi_{tj}$ distribution, albeit with the top quark and its balancing light jet both at relatively central rapidities. Also, the region to the right of the peak is dominantly comprised of events with a top quark back-to-back in azimuth with the leading light jet. In other words, the region close to and above $\Delta R_{tj} = \pi$ is filled by events with one resolved jet, and it is therefore described with NLO accuracy by the ST simulation, and LO accuracy by STJ. Once again, we see that the tuned MINLO Sudakov form factor in the STJ* simulation works as intended, with its prediction (red) falling within the $\lesssim 3\%$ uncertainty band of ST (green), and exceeding the ST central value by not more than 5%, across the region $\Delta R_{tj} \gtrsim \pi$.

The only way to populate the ΔR_{tj} region to the left of the peak is to have $\Delta\phi_{tj} < \pi$, moreover, the only way to populate $\Delta R_{tj} \lesssim 2\pi/3$ is with events in which the top quark recoils against more than two final-state objects. The latter description is, of course, familiar from the discussion on the $\Delta\phi_{tj}$ distribution just overhead, owing to the fact that, by definition, $\Delta R_{tj} \geq \Delta\phi_{tj}$. As a consequence, the NLO ST simulation is only LO accurate in the region $2\pi/3 \lesssim \Delta R_{tj} \lesssim \pi$, while it relies on the parton shower to fill $\Delta R_{tj} \lesssim 2\pi/3$. Conversely, the STJ simulation will be NLO accurate in the region $2\pi/3 \lesssim \Delta R_{tj} \lesssim \pi$, and LO below it. Once again, STJ* is seen to behave in the best possible way, moving away from the ST prediction on the peak at $\Delta R_{tj} \sim \pi$ and aligning exactly with the STJ result in the region below $\Delta R_{tj} \sim 2.6$.

Before moving on, we point out that the same $\Delta\phi_{tj}$ and ΔR_{tj} distributions seen here in figure 5 are reproduced for the 8 TeV LHC in appendix B (figure 10). These 8 TeV results display, quantitatively, exactly the same trends as those shown here, in particular they show the same excellent agreement between STJ* and ST/STJ simulations in the same regions of the plots elaborated on above. We emphasise that the 8 TeV STJ* predictions were obtained using the same neural network fit of the MINLO Sudakov form factor as employed for the plots in this section, suggesting that the fit comes with a reasonable degree of portability/universality.

3.7 Top transverse momentum in single jet events

In figure 6 we show how the top quark's transverse momentum spectrum, figure 2, is modified by requiring that it be accompanied by exactly one light jet. The distribution is plotted for two different jet transverse momentum thresholds: 25 GeV (left) and 100 GeV (right). The spectrum is of interest since the requirement to have only one light jet, in addition to the top quark, has been employed in event selections, as a means to reduce background, in LHC t-channel single-top analysis [26].

In both left- and right-hand plots of figure 6, in order to populate the region where the top quark's $p_{\text{T}}(t)$ is low with respect to the transverse momentum threshold at which jets are defined, and yet still have single-jet events, there must be a second collimated spray of radiation, to balance the transverse momentum. Hence, the events in this region are
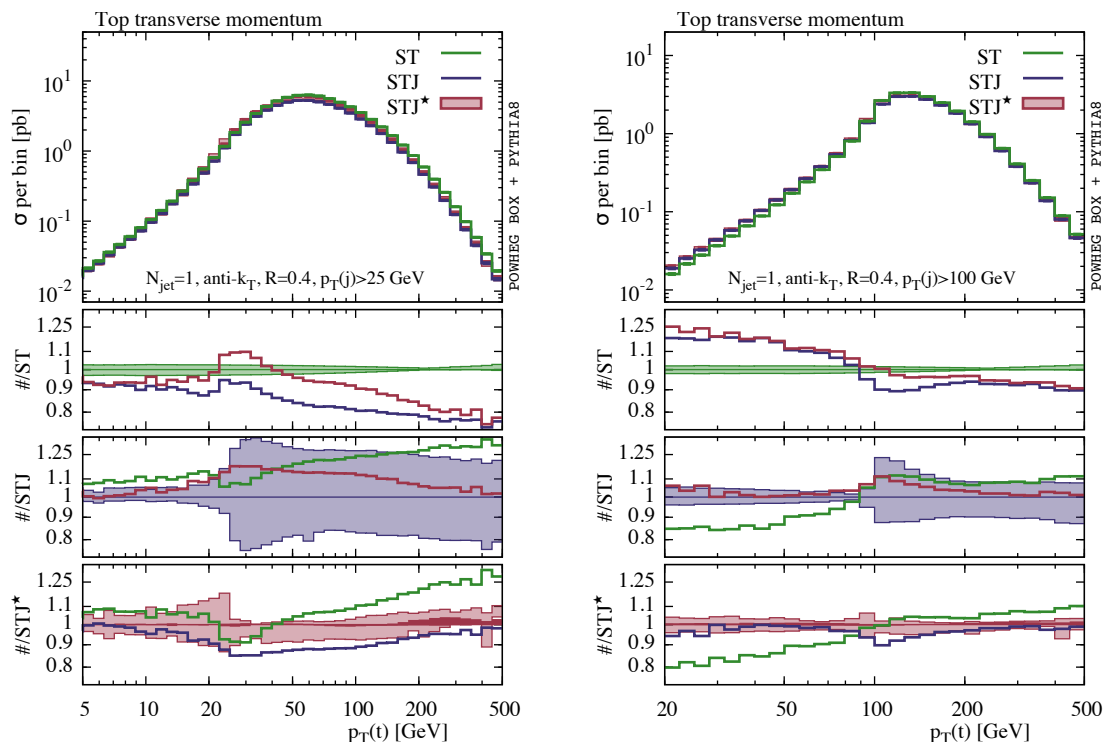
Figure 6. Transverse momentum of the top quark in events containing exactly one light $R = 0.4$ anti-k_t jet in addition to the top quark. On the left the distribution is defined with a 25 GeV jet transverse momentum threshold, while on the right-hand side a 100 GeV threshold is used. No other cuts are applied. All predictions follow the same colour conventions as figures 2–5.

expected to be two-jet like, with the resolved jet and its would-be-jet counterpart nearly back-to-back in azimuth as $p_{\rm T}(t) \to 0$ GeV. It follows that this region of $p_{\rm T}(t)$ is best described by the STJ program, with NLO accuracy, while the corresponding description in the ST program is LO. Being two-jet-like, the MINLO Sudakov form factor, tuned or not, will not act on these events, and so it is natural then to see STJ* (red) lie on top of STJ (blue), as we approach $p_{\rm T}(t) = 0$ GeV. The relative closeness of the ST prediction to the latter is consistent with it having LO accuracy in the same region.[17]

We now turn, temporarily, to consider the left-hand plot, wherein a 25 GeV jet transverse momentum threshold is in effect. If one looks to the high $p_{\rm T}(t)$ end, one is certainly considering a region dominated by large Sudakov logarithms, of sizeable ratios of scales $\sim Q_{bt}^2/p_{\rm T,cut}^2$ (eq. (2.6)), where $p_{\rm T,cut}$ denotes the jet transverse momentum threshold, at which the presence of a second radiated jet is vetoed. Thus, any variance (or lack of it), in the predictions for this tail of the spectrum, owes to differences in the Sudakov region around the $bq \to tq'$ underlying Born in each simulation.

In the peak of the distribution, $p_{\rm T}(t) \sim 50$ GeV, close to, but clearly above $p_{\rm T,cut}$, the make-up of the predictions, and our expectations for them, is less clear, owing to the complicated nature of the observable and the various dynamics which enter. We tentatively

---

[17]The smallness of the ST uncertainty band here is again an underestimate of the true theory uncertainty. It is a general feature in POWHEG NLOPS simulations, wherein the scale compensation associated with the NLO underlying Born kinematics, by default, is spread through all of the real radiation phase space.

suggest that the underlying Born configurations, $bq \rightarrow tq'$, associated with this region of the spectrum, are such that the 25 GeV transverse momentum veto on the presence of two or more jets, does not greatly restrict the phase space for radiation from those states. Assuming this to be the case, being inclusive w.r.t. radiation emitted from the underlying Born configurations, it is then not surprising to see the STJ prediction $\sim 10 - 20\%$ below the ST one in this region of the distribution. For the same reasons, the relative agreement of STJ* and ST in the same vicinity, is also anticipated, and desirable.

We suggest the same tentative explanations for the behaviour shown in the peak region of the right-hand $p_T(t)$ spectrum, as for that on the left. For the right-hand plot, however, the larger jet transverse momentum threshold of 100 GeV, means that the degree of integration over the phase space for additional radiation, at any given point in this region of the $p_T(t)$ spectrum, is more inclusive than in the case of the 25 GeV cut used for the left-hand plot. Hence, the STJ* prediction appears to follow that of ST over a slightly longer interval in the central region of the right-hand plot.

4 Conclusions

In this work we have developed a new NLO accurate simulation of t-channel single-top plus jet production, with matching to parton showers via the POWHEG method. The calculation has been carried out in the structure function approximation, wherein each of the fermion lines connected to the exchanged W-boson, and their associated radiative corrections, are treated as if they originated from two independent copies of the QCD sector (sections 2.1–2.2).

We have enhanced the NLO calculation underlying the simulation by applying a process-specific formulation of the MINLO method, as set out in section 2.3. The resulting STJ simulation yields NLO accuracy for t-channel single-top plus jet observables, and LO accuracy for inclusive t-channel single-top quantities (appendix A.1–A.2).

As well as producing a novel simulation for an important hadron collider process, our efforts have also concentrated significantly on the more general aim of improving and extending the MINLO method. To this end we have substantially evolved the proposal of ref. [79]. The latter article suggests that MINLO simulations can be made NLO accurate in describing both the original process on which the simulation was based, as well as that with one less jet, by fitting, approximately, unknown higher order terms in the MINLO Sudakov form factor to that effect. In this work we have applied the same idea. We postulate that the leading differences between the LO predictions of our STJ simulation and conventional NLO, for inclusive t-channel single-top production, owe to NNLL_σ terms in the MINLO Sudakov form factor that we do not control (section 2.4). We significantly improve on ref. [79] by fitting such an NNLL_σ correction to the Sudakov form factor directly in its exponent, rather than in its expansion. At the same time, we employ a more refined methodology in performing the fit, making use of advanced machine learning techniques for this purpose (section 2.5). The neural network machinery used in this part of our construction makes no assumptions regarding any dependence that the correction to the MINLO Sudakov form factor may have on the underlying Born kinematics, $bq \rightarrow tq'$, and it is given in terms of just 42 parameters, including weights and biases.

– 24 –

Our machine learning framework was applied to determine an approximate NNLL$_\sigma$ correction to the Minlo Sudakov form factor using $\mathcal{O}(20M)$ ST and STJ simulation events, produced for a 13 TeV LHC setup. The latter fitted term in our simulation is implemented as a small overall multiplicative correction to the weights of the events in the STJ Les Houches event files, which can be applied very quickly. We refer to this 'tuned' STJ simulation output, including the latter correction, as STJ*. The fit is performed seven times for correlated, factor-two, variations of the renormalization and factorization scales in the ST and STJ generators. In this way the STJ* predictions for inclusive t-channel single-top production yield very similar uncertainty estimates to those of the ST program, besides its central prediction.

The STJ and STJ* simulations were validated by comparing them to one another, and to the pre-existing ST Powheg program, for $\mathcal{O}(200)$ observables, at a 13 TeV LHC. This validation confirms well that the STJ predictions are LO accurate for inclusive t-channel single-top production, and NLO for the same process with an additional jet. The results also confirm that the improved STJ* simulation output is simultaneously NLO accurate for inclusive t-channel single-top and single-top plus jet processes. A representative selection of the distributions studied in our validation have been presented and discussed in section 3.

We have also carried out the same extensive analysis of observables assuming an 8 TeV LHC setup. For the latter we produced new ST, STJ and STJ* event samples accordingly. While it only takes 8-10 hours on a single CPU to generate a new Sudakov form factor fit for each scale choice, here in the STJ* simulation we continued to use the same fit obtained from 13 TeV LHC events, in order to test its universality. We find, again, that the STJ* predictions reproduce well the NLO accuracy of the ST program for inclusive t-channel single-top production observables. The latter observations are highly suggestive of a robustness and universality in the tuned Minlo Sudakov form factor. This is as one would expect, if the leading differences between the ST and STJ predictions for inclusive quantities are, as postulated, mostly/fully accounted for by missing higher order terms in the initial Minlo Sudakov form factor.

We advise, however, that if a tuning is carried out for a given collision energy and then used to reweight STJ events simulated at a much higher one, the enlarged $bq \to tq'$ phase space of the latter requires the neural network model to extrapolate outside the region covered by the data used to train it, e.g. into regions with very high transverse momentum or very high rapidity top quarks. One should therefore obviously not expect the neural network tunes to work so well when simulating STJ production at hadronic centre-of-mass energies significantly above those used in their training. For dedicated studies in such circumstances a new tuning of the Minlo Sudakov form factor can be carried out.

Finally, we point out that, given an NNLO calculation for t-channel single-top production, with the capability to compute distributions differential in the $bq \to tq'$ Born phase space, it is straightforward, in principle, to develop an NNLOPS simulation of this process using the methodology presented here.

The new STJ generator, together with the corresponding fits for promoting it to STJ*, will soon be publicly available in the Powheg Box V2 framework. While in this paper we have presented results only for single-top production, the code and the fits will be made available also for anti-top production.

Acknowledgments

A   MINLO supplement

In this appendix we give additional explanations and insights regarding key points of section 2.4, where we described how the accuracy of the new STJ program can be extended to NLO for ST observables. To this end, as with previous works on improving MINLO [69, 79] we compare the basic STJ cross section in section 2.3, differential in the underlying ST Born kinematics and the relevant radiation hardness parameter, to an analogous resummation formula. In appendix A.1 we describe a matched, resummed, cross section formula for the case at hand. Appendix A.2 compares the basic STJ simulation cross section to the latter, to clarify its accuracy for ST observables. Expanded explanation of our procedure for tuning the MINLO Sudakov form factor, such that the STJ code provides NLO descriptions of both t-channel single-top and t-channel single-top plus jet processes, is given in appendix A.3.

A.1   Resummation formula

Neglecting, momentarily, the top-quark mass, applying the CAESAR resummation formalism [89], the resummed cross section for the $1 \to 2$ exclusive k_t-jet rate, y_{12}, in single-top production, at next-to-leading log accuracy[18] (NLL_σ), with matching to NLO fixed order perturbation theory, can be written as

$$\frac{d\sigma_{\mathcal{RF}}}{d\Phi dy_{12}} = \frac{d\sigma_{\mathcal{R}}}{d\Phi dy_{12}} + \frac{d\sigma_{\mathcal{F}}}{d\Phi dy_{12}}, \qquad (A.1)$$

where $d\sigma_{\mathcal{F}}$ is a fixed order contribution, finite as $y_{12} \to 0$, and $d\sigma_{\mathcal{R}}$ embodies the all-orders resummation:

$$\frac{d\sigma_{\mathcal{R}}}{d\Phi dy_{12}} = \frac{d\sigma_{\mathrm{LO}}^{\mathrm{ST}}}{d\Phi} \left[1 + \bar{\alpha}_{\mathrm{S}} \bar{\chi}_1 (\Phi)\right] \frac{d}{dy_{12}} \left[\Delta(y_{12}) \prod_{\ell=1}^{n_i} \frac{q^{(\ell)}(x_\ell, y_{12})}{q^{(\ell)}(x_\ell, \mu_F^2)}\right]. \qquad (A.2)$$

---

[18]Resummation of terms of the form $\frac{1}{y_{12}} \bar{\alpha}_{\mathrm{S}}^n \ln^m \frac{Q}{y_{12}}$, with $m = 2n - 1$ and $m = 2n - 2$.

The first factor in eq. (A.2), $d\sigma_{\mathrm{LO}}^{\mathrm{ST}}/d\Phi$, denotes the leading order cross section for single-top production, fully differential in its associated kinematics, Φ. The $\bar{\chi}_1(\Phi)$ term encodes hard virtual next-to-leading order corrections to $d\sigma_{\mathrm{LO}}^{\mathrm{ST}}/d\Phi$ such that

$$\frac{d\sigma_{\mathrm{NLO}}^{\mathrm{ST}}}{d\Phi} = \frac{d\sigma_{\mathrm{LO}}^{\mathrm{ST}}}{d\Phi} \left[1 + \bar{\alpha}_{\mathrm{S}} \bar{\chi}_1(\Phi) \right] + \int dy_{12} \frac{d\sigma_{\mathcal{F}}}{d\Phi dy_{12}}, \tag{A.3}$$

$$\frac{d\sigma_{\mathcal{F}}}{d\Phi dy_{12}} = \frac{d\sigma_{\mathrm{LO}}^{\mathrm{STJ}}}{d\Phi dy_{12}} - \frac{d\sigma_{\mathcal{R},1}}{d\Phi dy_{12}}\bigg|_{\bar{\chi}_1 \to 0}, \tag{A.4}$$

where $d\sigma_{\mathcal{R},1}$ denotes the α_{S} expansion of $d\sigma_{\mathcal{R}}$. The $q^{(\ell)}(x_\ell, \mu^2)$ factors are parton distribution functions (PDFs), for a given incoming leg, ℓ, evaluated at momentum fraction x_ℓ, and scale μ. The product of PDF ratios runs over $n_i = 2$ incoming legs. Except for the argument of α_{S} in the integrands of $\Delta(y_{12})$, renormalization and factorization scales are set to a hard scale characteristic of the leading order single-top production process throughout eqs. (A.1–A.4).

In neglecting the top-quark mass to use the CAESAR framework, the various elements of eqs. (A.2)–(A.4) should be initially understood as defined in the $m_t \to 0$ limit. Extrapolating eq. (A.2) to include the finite top-mass is then straightforward, involving no change to the form of eqs. (A.2)–(A.4) but rather just obvious extensions of the elements making them up.

Being in the final-state, the top quark, whether we neglect its mass or not, does not affect the PDF dependence of eq. (A.2). The Sudakov form factor exponent, on the other hand, must be supplemented by a set terms which vanish in the $m_t \to 0$ limit (eq. (2.5)), i.e. $\Delta(y_{12})$ in eq. (A.2) should be hence understood as the full expression in eq. (2.3) rather than its $m_t \to 0$ limit. We remind again that the latter finite quark mass extension of the Sudakov form factor is identical to that in eq. 10 of the k_t-jet rate resummation of ref. [104]. The only other modification to the resummed expression in eq. (A.2), due to the finite top mass, is trivial, merely consisting of henceforth understanding that $d\sigma_{\mathrm{LO}}^{\mathrm{ST}}$ and $d\sigma_{\mathrm{NLO}}^{\mathrm{ST}}$ refer to the LO and NLO single-top cross sections with the full top-mass dependence. The fixed order matching terms $\bar{\chi}_1$ and $d\sigma_{\mathcal{F}}$ remain determined by eq. (A.3), subject to the latter modifications.

A.2 STJ predictions for ST observables

Here we compare the resummed and matched cross section of eq. (A.1) to that of STJ, to better understand its predictions for inclusive t-channel single-top observables, since we know what these are in the case of eq. (A.1). To this end we first recast $d\sigma_{\mathcal{RF}}$ (eq. (A.1)) in the same form as the STJ cross section $d\sigma_{\mathrm{STJ}}^{\mathcal{M}}$ (eq. (2.1)). With no approximations we can rewrite $d\sigma_{\mathcal{R}}$ in eq. (A.2) as

$$\frac{d\sigma_{\mathcal{R}}}{d\Phi dy_{12}} = \Delta(y_{12}) \frac{d\sigma_{\mathrm{LO}}^{\mathrm{ST}}}{d\Phi} \left[1 + \bar{\alpha}_{\mathrm{S}} \bar{\chi}_1(\Phi) \right] \frac{d}{dy_{12}} \ln \left[\Delta(y_{12}) \prod_{\ell=1}^{n_i} q^{(\ell)}(x_\ell, y_{12}) \right], \tag{A.5}$$

wherein the renormalization and factorization scales are now set to $\sqrt{y_{12}}$ throughout, save for those in the integrands of $\Delta(y_{12})$, which remain evaluated at q, as set out in section 2.3.

Neglecting $\mathcal{O}(\alpha_{\mathrm{S}}^2)$ terms which are finite as $y_{12} \to 0$, we introduce a factor $\Delta(y_{12})\,[1+\bar{\alpha}_{\mathrm{S}}\bar{\chi}_1]$ in front of $d\sigma_{\mathcal{F}}$ in eq. (A.1), setting $\mu_R = \mu_F = \sqrt{y_{12}}$ throughout that term. Taken together with eq. (A.5), this gives, via eq. (A.4), without further approximation,

$$\frac{d\sigma_{\mathcal{RF}}}{d\Phi dy_{12}} = \Delta(y_{12}) \left[\frac{d\sigma_{\mathrm{NLO}}^{\mathrm{APX}}}{d\Phi dy_{12}} - \Delta(y_{12})|_{\bar{\alpha}_{\mathrm{S}}} \frac{d\sigma_{\mathrm{LO}}^{\mathrm{STJ}}}{d\Phi dy_{12}} \right], \tag{A.6}$$

$$\frac{d\sigma_{\mathrm{NLO}}^{\mathrm{APX}}}{d\Phi dy_{12}} = \frac{d\sigma_{\mathrm{LO}}^{\mathrm{STJ}}}{d\Phi dy_{12}} \left[1 + \Delta(y_{12})|_{\bar{\alpha}_{\mathrm{S}}} + \bar{\alpha}_{\mathrm{S}}\bar{\chi}_1(\Phi) \right]. \tag{A.7}$$

Since the aforementioned neglected $\mathcal{O}(\alpha_{\mathrm{S}}^2)$ terms are finite as $y_{12} \to 0$, eq. (A.6) is completely unchanged with respect to eq. (A.1) in regards to the logarithmic terms $\propto 1/y_{12}$, and so too is its fixed order accuracy up to and including terms of $\mathcal{O}(\alpha_{\mathrm{S}})$. This is the case both in the cumulant cross section and the y_{12} spectrum. This means, in particular, that $d\sigma_{\mathcal{RF}}/d\Phi$ remains equal to $d\sigma_{\mathrm{NLO}}^{\mathrm{ST}}/d\Phi$ up to $\mathcal{O}(\alpha_{\mathrm{S}}^2)$ unenhanced terms.

To ease comparison, we write again here the STJ formula, eq. (2.1), differential in Φ and y_{12},

$$\frac{d\sigma_{\mathcal{M}}}{d\Phi dy_{12}} = \Delta(y_{12}) \left[\frac{d\sigma_{\mathrm{NLO}}^{\mathrm{STJ}}}{d\Phi dy_{12}} - \Delta(y_{12})|_{\bar{\alpha}_{\mathrm{S}}} \frac{d\sigma_{\mathrm{LO}}^{\mathrm{STJ}}}{d\Phi dy_{12}} \right]. \tag{A.8}$$

The difference between eqs. (A.6) and (A.8) is clearly limited to the first term in each of the square brackets in $d\sigma_{\mathrm{NLO}}^{\mathrm{APX}}$ and $d\sigma_{\mathrm{NLO}}^{\mathrm{STJ}}$. Now let's zoom in on this.

Suppressing, for brevity, the $d\Phi\,dy_{12}$'s, and dropping terms beyond NLL_σ accuracy, we can write $d\sigma_{\mathcal{RF}} = \Delta(y_{12})\,d\sigma_{\mathrm{LO}}^{\mathrm{STJ}}$, whereupon it follows that exactly to $\mathcal{O}(\alpha_{\mathrm{S}})$, and to NLL_σ accuracy at $\mathcal{O}(\alpha_{\mathrm{S}}^2)$, $d\sigma_{\mathrm{NLO}}^{\mathrm{APX}}$ is the same as $d\sigma_{\mathrm{NLO}}^{\mathrm{STJ}}$, i.e.

$$d\sigma_{\mathrm{NLO}}^{\mathrm{STJ}} = d\sigma_{\mathrm{NLO}}^{\mathrm{APX}} + d\sigma_{\mathrm{NLO}}^{\mathrm{RES}}, \qquad d\sigma_{\mathrm{NLO}}^{\mathrm{RES}} = \frac{d\sigma_{\mathrm{LO}}^{\mathrm{STJ}}}{d\Phi dy_{12}} \bar{\alpha}_{\mathrm{S}}\,\mathcal{C}_{21} + \mathcal{O}(\alpha_{\mathrm{S}}^2/y_{12}), \tag{A.9}$$

where $\mathcal{C}_{21}$ is a Φ-dependent $\mathcal{O}(1)$ coefficient that we do not presume to know. Inserting eq. (A.9) into eq. (A.8) and integrating over y_{12} yields

$$\frac{d\sigma_{\mathcal{M}}}{d\Phi} - \frac{d\sigma_{\mathcal{RF}}}{d\Phi} = \frac{d\sigma_{\mathrm{LO}}^{\mathrm{ST}}}{d\Phi} \cdot \mathcal{O}(\alpha_{\mathrm{S}}), \tag{A.10}$$

with the $\mathcal{O}(\alpha_{\mathrm{S}})$ ambiguity due to the leading (unknown) NNLL_σ term in $\Delta(y_{12})\,d\sigma_{\mathrm{NLO}}^{\mathrm{RES}}$. Since $d\sigma_{\mathcal{RF}}/d\Phi$ is NLO accurate, eq. (A.10) means that the standard STJ calculation in section 2.3, has only LO accuracy for inclusive t-channel single-top observables. The numerical comparisons in section 3, between POWHEG ST and STJ simulations, give strong numerical support to the analysis here.

A.3 STJ → STJR*

While we do not in general control NNLL_σ terms, it's clear that $d\sigma_{\mathrm{NLO}}^{\mathrm{STJ}}$ also includes the process-dependent $\bar{\alpha}_{\mathrm{S}}\bar{\chi}_1(\Phi)$ term of $d\sigma_{\mathrm{NLO}}^{\mathrm{APX}}$, owing to the ST hard virtual corrections implicit in the soft-collinear limit of the NLO STJ cross section. With the latter point in mind, we postulate that any NNLL_σ extension of the resummed, matched, cross section formula, $d\sigma_{\mathcal{RF}}$, in section A.1, would have exactly the same form as in eq. (A.1) (or be may be re-expressed as such), with the only difference being the inclusion of NNLL_σ terms in

the Sudakov form factor exponent. The latter modification is exactly what previous works on improving MINLO in the context of other processes would advocate [69, 79, 93, 94], as well as the general CAESAR resummation formalism for processes involving only massless partons.

In the presence of such a modification the fixed order properties of $d\sigma_{\mathcal{RF}}$ are unaltered. The $\mathcal{O}(\alpha_{\mathrm{S}})$ radiation spectrum of eq. (A.1) with respect to the ST Born kinematics is unchanged by the introduction of $\mathcal{O}(\alpha_{\mathrm{S}}^2)$ terms in the Sudakov exponent, and it is trivially still the case that $d\sigma_{\mathcal{RF}}/d\Phi = d\sigma_{\mathrm{NLO}}^{\mathrm{ST}}/d\Phi$. The form of the STJ cross section is also completely unchanged with respect to eqs. (2.1) and (A.8).

Since the STJ cross section is accurate to $\mathcal{O}(\alpha_{\mathrm{S}}^2)$ in the y_{12} spectrum, if the resummation formula with the modified Sudakov form factor is NNLL_σ accurate, then it must reproduce all NNLL_σ terms in the latter on expansion in α_{S}. It follows that the result of such a change in $\Delta(y_{12})$ in section A.2, is to reduce the residual difference between $d\sigma_{\mathrm{NLO}}^{\mathrm{STJ}}$ and its counterpart, $d\sigma_{\mathrm{NLO}}^{\mathrm{APX}}$, in the resummation formula, eq. (A.6):

$$\frac{d\sigma_{\mathrm{NLO}}^{\mathrm{APX}}}{d\Phi dy_{12}} \rightarrow \frac{d\sigma_{\mathrm{LO}}^{\mathrm{STJ}}}{d\Phi dy_{12}} \left[1 + \Delta(y_{12})|_{\bar{\alpha}_{\mathrm{S}}} + \bar{\alpha}_{\mathrm{S}} \left[\bar{\chi}_1(\Phi) + \mathcal{C}_{21}(\Phi) \right] \right] , \tag{A.11}$$

$$d\sigma_{\mathrm{NLO}}^{\mathrm{RES}} \rightarrow \frac{d\sigma_{\mathrm{LO}}^{\mathrm{ST}}}{d\Phi} \frac{\mathcal{C}_{20}(\Phi)}{y_{12}} \bar{\alpha}_{\mathrm{S}}^2 + \mathcal{O}(\alpha_{\mathrm{S}}^2) . \tag{A.12}$$

Combining eqs. (A.11)–(A.12) with eqs. (A.6), (A.8), (A.9) and integrating over y_{12} then quickly yields

$$\frac{d\sigma_{\mathcal{M}}}{d\Phi} - \frac{d\sigma_{\mathcal{RF}}}{d\Phi} = \frac{d\sigma_{\mathrm{LO}}^{\mathrm{ST}}}{d\Phi} \cdot \mathcal{O}(\alpha_{\mathrm{S}}^{3/2}) . \tag{A.13}$$

From here it is then clear that if the coefficient of the suggested NNLL_σ term in the Sudakov form factor was further modified by a suitably defined, spurious, formally subleading term, $\sim 1 + \mathcal{O}(\sqrt{\alpha_{\mathrm{S}}})$, we can arrange that

$$\frac{d\sigma_{\mathcal{M}}}{d\Phi} = \frac{d\sigma_{\mathcal{RF}}}{d\Phi} = \frac{d\sigma_{\mathrm{NLO}}^{\mathrm{ST}}}{d\Phi} . \tag{A.14}$$

Assuming our postulate is valid, namely, that promoting eq. (A.1) from NLL_σ to NNLL_σ accuracy amounts to including a missing term in the Sudakov form factor of the form

$$\ln \delta\Delta(y_{12}) = -\int_{y_{12}}^{Q_{bt}^2} \frac{dq^2}{q^2} \bar{\alpha}_{\mathrm{S}}^2 \mathcal{A}_2(\Phi) \ln \frac{Q_{bt}^2}{q^2} , \tag{A.15}$$

then we may determine the unknown $\mathcal{A}_2(\Phi)$ therein, up to a factor $\sim 1 + \mathcal{O}(\sqrt{\alpha_{\mathrm{S}}})$, by fitting it such that eq. (A.14) is satisfied. The resulting improved STJ cross section, $\mathrm{STJ}^\star$, will then converge on the NNLL_σ resummation while remaining NLO accurate for STJ observables, and further acquiring NLO accuracy for inclusive ST ones.

While we assume a form for the resummation formula at NNLL_σ, we do not presume to know the details of the related Sudakov ingredients at that order, so we allow the $\mathcal{A}_2$ coefficient to have a general dependence on Φ already for this reason alone. If the true NNLL_σ resummation turned out to be Φ-independent, this should be reflected by a relative flatness of the fitted $\mathcal{A}_2(\Phi)$. However, even if this is the case at NNLL_σ, the relative $\mathcal{O}(\sqrt{\alpha_{\mathrm{S}}})$

ambiguity on the fitted $\mathcal{A}_2$, also absorbs the effects of unknown $\mathrm{N^3LL}_\sigma$ Sudakov terms, which are established as having a general dependence on the Born kinematics in so-called process-dependent resummation formulae like that of MINLO (see e.g. [69, 94, 105]). While formally subleading, it is well known that such $\mathrm{N^3LL}_\sigma$ Sudakov terms can be large [106]. Furthermore, besides $\mathrm{N^3LL}_\sigma$ ambiguities, also spurious, finite, non-logarithmic $\mathcal{O}(\alpha_\mathrm{s}^2)$ terms in STJ can contribute Φ-dependent differences between $d\sigma_\mathcal{M}/d\Phi$ and $d\sigma_\mathrm{NLO}^{\mathrm{ST}}/d\Phi$. Given these reasons, together with the fact that the primary objective is to render the STJ simulation NLO accurate for both t-channel single-top and t-channel single-top plus jet observables, we allow for a general dependence on Φ in the fitted $\mathcal{A}_2$ coefficient.

If our postulate is correct then the fitted quantity we obtain, being of Sudakov origin, will be universal to NNLL_σ accuracy. Moreover, if the leading $\mathcal{O}(\sqrt{\alpha_\mathrm{s}})$ ambiguity in that fitted coefficient is also completely due to a deficiency in the MINLO Sudakov, at $\mathrm{N^3LL}_\sigma$, that too will be universal; more specifically, it should not depend on the collider centre-of-mass energy or the PDFs. That hypothesis has support from the fact that, in all earlier work, the inclusion of higher order terms in the Sudakov form factor has been all that was required to promote MINLO simulations of jet-associated production processes to NLO accuracy for their inclusive analogues [69, 79, 93, 94]. If true, $\mathcal{A}_2$ fits performed for a given collider setup would formally maintain the equality in eq. (A.14) up to $\mathcal{O}(\alpha_\mathrm{s}^2)$ terms when used in the context of other setups, e.g. with different centre-of-mass energies and/or different PDFs. So, while the fits performed in this paper correspond to a specific 13 TeV LHC setup, we expect that, in practice, they should be somewhat robust against changes to it. This is exactly what we find when using the fits for generating 8 TeV results, see appendix B. We advise, however, that, in general, if a fit is carried out for some given collision energy and then used to reweight STJ events simulated at a much higher one, the enlarged phase space of the latter means that the neural network model will need to interpolate outside the region covered by the data used to train it, e.g. in regions with very high transverse momentum/rapidity top quarks. Hence, we expect our approach to work well provided the neural network Sudakov form factor tuning is not applied when simulating STJ production at energies significantly above that used in its training.

B MINLO fit extrapolation from 13 TeV to 8 TeV

In this appendix we show a representative sub-sample of the distributions presented in the main text for the 13 TeV LHC, here, instead, for the 8 TeV LHC. The purpose of the presentation is to give an indication as to how well the tuned MINLO Sudakov form factor in STJ*, obtained by carrying out the neural network fitting procedure (section 2.5) using 13 TeV ST and STJ events, can perform under different running conditions to those used for training the network.

To further gauge the universality of the output of the Sudakov form factor tuning procedure, the red and orange lines in the plots of this subsection compare 8 TeV predictions obtained with a STJ* simulation, tuned on 13 TeV event samples, (red), to those of a STJ* simulation tuned on the same 8 TeV event samples (orange) used to make the ST, (green), and STJ, (blue), results. In general we observe a remarkable level of agreement in the predictions obtained with the two different STJ* tunes.
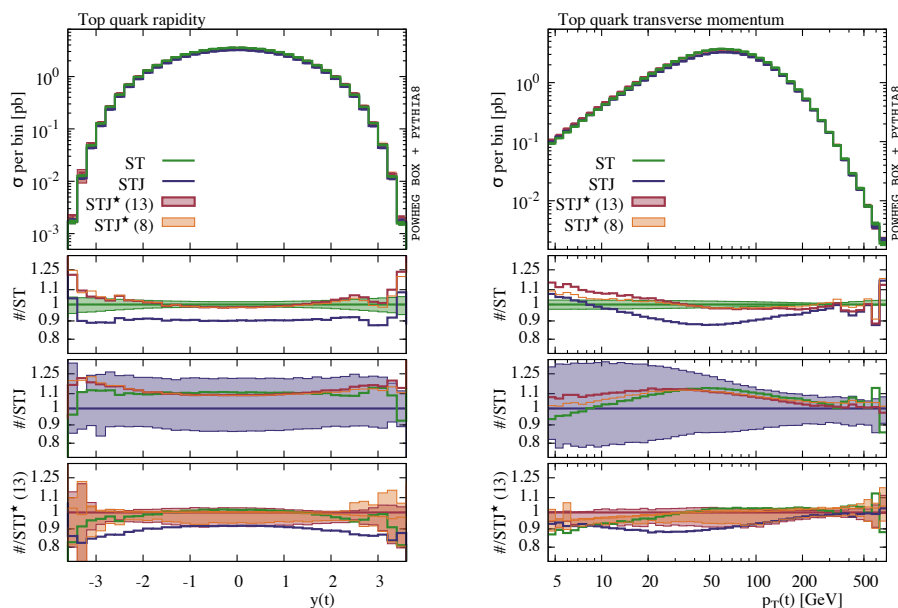
Figure 7. Here we show the same predictions as in figure 2, but for an 8 TeV rather than a 13 TeV LHC. The left-hand plot shows the rapidity of the top quark in t-channel single-top production, while the right-hand plot shows its transverse momentum. As with the STJ* predictions in the main text, the STJ* (13) predictions (red) are obtained by tuning the MINLO Sudakov form factor using 13 TeV LHC ST and STJ event samples. The STJ* (8) predictions (orange) are obtained by tuning the MINLO Sudakov form factor using 8 TeV LHC ST and STJ event samples. The very good level of agreement between STJ* (13) and STJ* (8) predictions points to a high degree of universality in the Sudakov form factor corrections output by the tuning procedure.
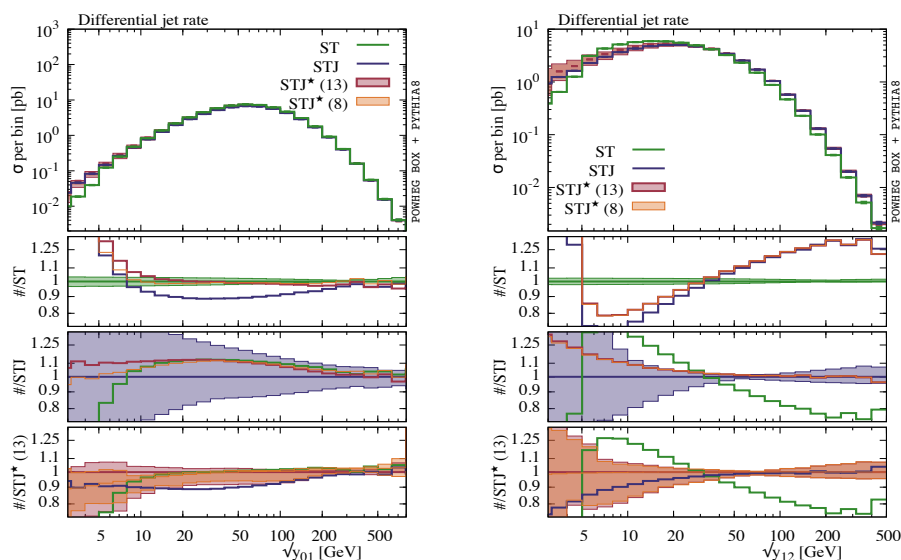
Figure 8. $0 \to 1$ (left) and $1 \to 2$ (right) differential jet rates in the k_t clustering algorithm, at the 8 TeV LHC. As in figure 7, the STJ* (13) program (red) uses a MINLO Sudakov form factor tuned using 13 TeV LHC ST and STJ samples, according to sections 2.4–2.5. The STJ* (8) program analogously uses a MINLO Sudakov form factor tuned with 8 TeV LHC ST and STJ samples.
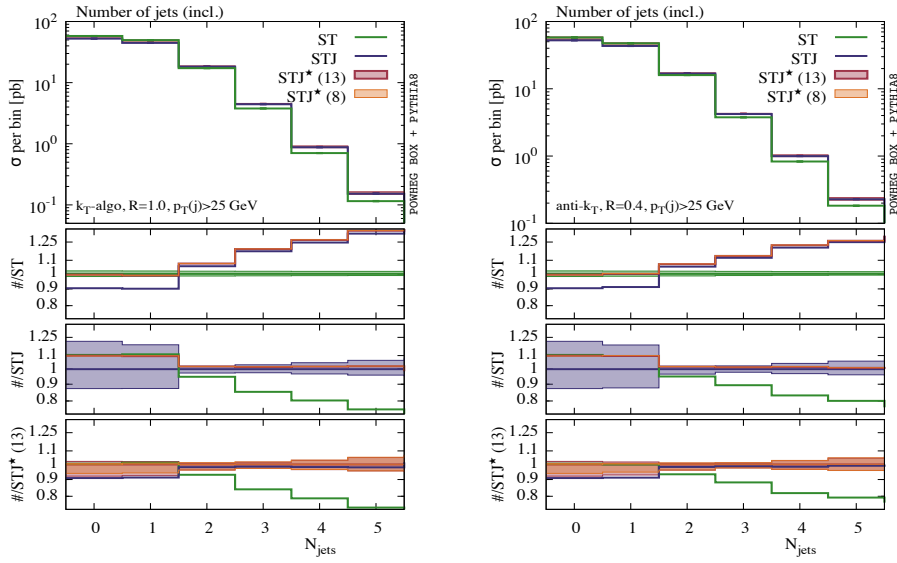
Figure 9. Inclusive jet cross sections at the 8 TeV LHC. The left-hand plot shows predictions for jets defined according to the k_t clustering algorithm with radius parameter $R = 1$. The right-hand plot gives predictions for the anti-k_t algorithm with $R = 0.4$. The STJ* (13) program (red) uses a MINLO Sudakov form factor tuned using 13 TeV LHC ST and STJ events (sections 2.4–2.5). The STJ* (8) program uses a MINLO Sudakov form factor tuned with 8 TeV LHC ST and STJ events.
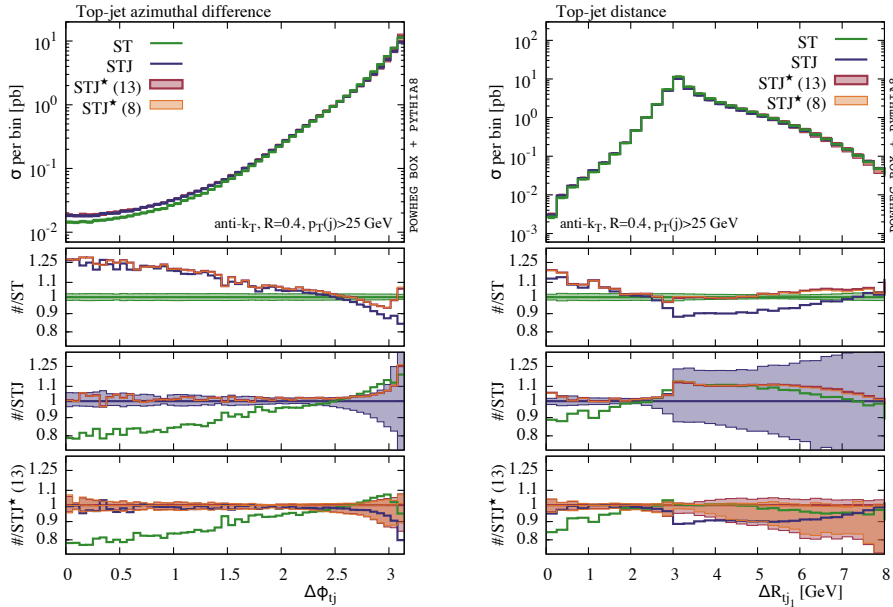
Figure 10. The left-hand plot shows predictions for the azimuthal angle between the top quark and the leading jet in t-channel single-top production at the 8 TeV LHC. The right-hand plot similarly shows predictions for the distance between the same two objects in the $\eta - \phi$ plane. The colour coding and naming of the various predictions is as in figures 7–9.

References

[1] P.W. Higgs, *Broken symmetries and the masses of gauge bosons*, *Phys. Rev. Lett.* **13** (1964) 508 [INSPIRE].

[2] F. Englert and R. Brout, *Broken symmetry and the mass of gauge vector mesons*, *Phys. Rev. Lett.* **13** (1964) 321 [INSPIRE].

[3] W. Bernreuther, *Top quark physics at the LHC*, *J. Phys.* **G 35** (2008) 083001 [arXiv:0805.1333] [INSPIRE].

[4] M. Cacciari et al., *Top-pair production at hadron colliders with next-to-next-to-leading logarithmic soft-gluon resummation*, *Phys. Lett.* **B 710** (2012) 612 [arXiv:1111.5869] [INSPIRE].

[5] M. Czakon and A. Mitov, *Top++: a program for the calculation of the top-pair cross-section at hadron colliders*, *Comput. Phys. Commun.* **185** (2014) 2930 [arXiv:1112.5675] [INSPIRE].

[6] M. Czakon, P. Fiedler and A. Mitov, *Total top-quark pair-production cross section at hadron colliders through $O(\alpha_S^4)$*, *Phys. Rev. Lett.* **110** (2013) 252004 [arXiv:1303.6254] [INSPIRE].

[7] M. Czakon et al., *Top-pair production at the LHC through NNLO QCD and NLO EW*, *JHEP* **10** (2017) 186 [arXiv:1705.04105] [INSPIRE].

[8] M. Aliev et al., *HATHOR: HAdronic Top and Heavy quarks crOss section calculatoR*, *Comput. Phys. Commun.* **182** (2011) 1034 [arXiv:1007.1327] [INSPIRE].

[9] P. Kant et al., *HatHor for single top-quark production: updated predictions and uncertainty estimates for single top-quark production in hadronic collisions*, *Comput. Phys. Commun.* **191** (2015) 74 [arXiv:1406.4403] [INSPIRE].

[10] N. Kidonakis, *Two-loop soft anomalous dimensions for single top quark associated production with a W^- or H^-*, *Phys. Rev.* **D 82** (2010) 054018 [arXiv:1005.4451] [INSPIRE].

[11] N. Kidonakis, *Top quark production*, in the proceedings of the *Helmholtz International Summer School on Physics of Heavy Quarks and Hadrons (HQ 2013)*, July 15–28, JINR, Dubna, Russia (2014), arXiv:1311.0283.

[12] J. Alwall et al., *Is $V_{(tb)} \simeq 1$?*, *Eur. Phys. J.* **C 49** (2007) 791 [hep-ph/0607115] [INSPIRE].

[13] H. Lacker et al., *Model-independent extraction of $|V_{tq}|$ matrix elements from top-quark measurements at hadron colliders*, *Eur. Phys. J.* **C 72** (2012) 2048 [arXiv:1202.4694] [INSPIRE].

[14] Q.-H. Cao, B. Yan, J.-H. Yu and C. Zhang, *A general analysis of W_{tb} anomalous couplings*, *Chin. Phys.* **C 41** (2017) 063101 [arXiv:1504.03785] [INSPIRE].

[15] E. Alvarez, L. Da Rold, M. Estevez and J.F. Kamenik, *Measuring $|V_{td}|$ at the LHC*, *Phys. Rev.* **D 97** (2018) 033002 [arXiv:1709.07887] [INSPIRE].

[16] T.M.P. Tait and C.P. Yuan, *Single top quark production as a window to physics beyond the standard model*, *Phys. Rev.* **D 63** (2000) 014018 [hep-ph/0007298] [INSPIRE].

[17] Q.-H. Cao, J. Wudka and C.P. Yuan, *Search for new physics via single top production at the LHC*, *Phys. Lett.* **B 658** (2007) 50 [arXiv:0704.2809] [INSPIRE].

[18] D. Atwood, S. Bar-Shalom, G. Eilam and A. Soni, *CP violation in top physics*, *Phys. Rept.* **347** (2001) 1 [hep-ph/0006032] [INSPIRE].

[19] E. Drueke et al., *Single top production as a probe of heavy resonances*, *Phys. Rev.* **D 91** (2015) 054020 [arXiv:1409.7607] [INSPIRE].

[20] J.A. Aguilar-Saavedra, C. Degrande and S. Khatibi, *Single top polarisation as a window to new physics*, *Phys. Lett.* **B 769** (2017) 498 [arXiv:1701.05900] [INSPIRE].

[21] C. Zhang, *Single top production at next-to-leading order in the standard model effective field theory*, *Phys. Rev. Lett.* **116** (2016) 162002 [arXiv:1601.06163] [INSPIRE].

[22] ATLAS collaboration, *Measurement of the t-channel single top-quark production cross section in pp collisions at $\sqrt{s} = 7$ TeV with the ATLAS detector*, *Phys. Lett.* **B 717** (2012) 330 [arXiv:1205.3130] [INSPIRE].

[23] ATLAS collaboration, *Comprehensive measurements of t-channel single top-quark production cross sections at $\sqrt{s} = 7$ TeV with the ATLAS detector*, *Phys. Rev.* **D 90** (2014) 112006 [arXiv:1406.7844] [INSPIRE].

[24] ATLAS collaboration, *Search for anomalous couplings in the W_{tb} vertex from the measurement of double differential angular decay rates of single top quarks produced in the t-channel with the ATLAS detector*, *JHEP* **04** (2016) 023 [arXiv:1510.03764] [INSPIRE].

[25] ATLAS collaboration, *Measurement of the inclusive cross-sections of single top-quark and top-antiquark t-channel production in pp collisions at $\sqrt{s} = 13$ TeV with the ATLAS detector*, *JHEP* **04** (2017) 086 [arXiv:1609.03920] [INSPIRE].

[26] ATLAS collaboration, *Fiducial, total and differential cross-section measurements of t-channel single top-quark production in pp collisions at 8 TeV using data collected by the ATLAS detector*, *Eur. Phys. J.* **C 77** (2017) 531 [arXiv:1702.02859] [INSPIRE].

[27] ATLAS collaboration, *Probing the W_{tb} vertex structure in t-channel single-top-quark production and decay in pp collisions at $\sqrt{s} = 8$ TeV with the ATLAS detector*, *JHEP* **04** (2017) 124 [arXiv:1702.08309] [INSPIRE].

[28] CMS collaboration, *Measurement of the t-channel single top quark production cross section in pp collisions at $\sqrt{s} = 7$ TeV*, *Phys. Rev. Lett.* **107** (2011) 091802 [arXiv:1106.3052] [INSPIRE].

[29] CMS collaboration, *Measurement of the single-top-quark t-channel cross section in pp collisions at $\sqrt{s} = 7$ TeV*, *JHEP* **12** (2012) 035 [arXiv:1209.4533] [INSPIRE].

[30] CMS collaboration, *Measurement of the t-channel single-top-quark production cross section and of the $|V_{tb}|$ CKM matrix element in pp collisions at $\sqrt{s} = 8$ TeV*, *JHEP* **06** (2014) 090 [arXiv:1403.7366] [INSPIRE].

[31] CMS collaboration, *Measurement of top quark polarisation in t-channel single top quark production*, *JHEP* **04** (2016) 073 [arXiv:1511.02138] [INSPIRE].

[32] CMS collaboration, *Cross section measurement of t-channel single top quark production in pp collisions at $\sqrt{s} = 13$ TeV*, *Phys. Lett.* **B 772** (2017) 752 [arXiv:1610.00678] [INSPIRE].

[33] CMS collaboration, *Search for anomalous W_{tb} couplings and flavour-changing neutral currents in t-channel single top quark production in pp collisions at $\sqrt{s} = 7$ and 8 TeV*, *JHEP* **02** (2017) 028 [arXiv:1610.03545] [INSPIRE].

[34] CMS collaboration, *Measurement of the top quark mass using single top quark events in proton-proton collisions at* $\sqrt{s} = 8\,TeV$, *Eur. Phys. J.* **C 77** (2017) 354 [arXiv:1703.02530] [inSPIRE].

[35] A. Giammanco, *Single top quark production at the LHC*, *Rev. Phys.* **1** (2016) 1 [arXiv:1511.06748] [inSPIRE].

[36] A. Giammanco and R. Schwienhorst, *Single top-quark production at the Tevatron and the LHC*, *Rev. Mod. Phys.* **90** (2018) 035001 [arXiv:1710.10699] [inSPIRE].

[37] B.W. Harris et al., *The fully differential single top quark cross-section in next to leading order QCD*, *Phys. Rev.* **D 66** (2002) 054024 [hep-ph/0207055] [inSPIRE].

[38] J.M. Campbell, R.K. Ellis and F. Tramontano, *Single top production and decay at next-to-leading order*, *Phys. Rev.* **D 70** (2004) 094012 [hep-ph/0408158] [inSPIRE].

[39] Q.H. Cao et al., *Next-to-leading order corrections to single top quark production and decay at the Tevatron: 2. t^- channel process*, *Phys. Rev.* **D 72** (2005) 094027 [hep-ph/0504230] [inSPIRE].

[40] J.M. Campbell, R. Frederix, F. Maltoni and F. Tramontano, *Next-to-leading-order predictions for t-channel single-top production at hadron colliders*, *Phys. Rev. Lett.* **102** (2009) 182003 [arXiv:0903.0005] [inSPIRE].

[41] J.M. Campbell, R. Frederix, F. Maltoni and F. Tramontano, *NLO predictions for t-channel production of single top and fourth generation quarks at hadron colliders*, *JHEP* **10** (2009) 042 [arXiv:0907.3933] [inSPIRE].

[42] J.M. Campbell and R.K. Ellis, *Top-quark processes at NLO in production and decay*, *J. Phys.* **G 42** (2015) 015005 [arXiv:1204.1513] [inSPIRE].

[43] M. Brucherseifer, F. Caola and K. Melnikov, *On the NNLO QCD corrections to single-top production at the LHC*, *Phys. Lett.* **B 736** (2014) 58 [arXiv:1404.7116] [inSPIRE].

[44] E.L. Berger, J. Gao, C.P. Yuan and H.X. Zhu, *NNLO QCD corrections to t-channel single top-quark production and decay*, *Phys. Rev.* **D 94** (2016) 071501 [arXiv:1606.08463] [inSPIRE].

[45] E.L. Berger, J. Gao and H.X. Zhu, *Differential distributions for t-channel single top-quark production and decay at next-to-next-to-leading order in QCD*, *JHEP* **11** (2017) 158 [arXiv:1708.09405] [inSPIRE].

[46] J. Wang, C.S. Li, H.X. Zhu and J.J. Zhang, *Factorization and resummation of t-channel single top quark production*, arXiv:1010.4509 [inSPIRE].

[47] N. Kidonakis, *Next-to-next-to-leading-order collinear and soft gluon corrections for t-channel single top quark production*, *Phys. Rev.* **D 83** (2011) 091503 [arXiv:1103.2792] [inSPIRE].

[48] Q.-H. Cao et al., *Transverse momentum resummation for t-channel single top quark production at the LHC*, arXiv:1801.09656 [inSPIRE].

[49] S. Frixione, E. Laenen, P. Motylinski and B.R. Webber, *Single-top production in MC@NLO*, *JHEP* **03** (2006) 092 [hep-ph/0512250] [inSPIRE].

[50] S. Frixione et al., *Single-top hadroproduction in association with a W boson*, *JHEP* **07** (2008) 029 [arXiv:0805.3067] [inSPIRE].

[51] R. Frederix, E. Re and P. Torrielli, *Single-top t-channel hadroproduction in the four-flavour scheme with POWHEG and aMC@NLO*, *JHEP* **09** (2012) 130 [arXiv:1207.5391] [inSPIRE].

[52] S. Alioli, P. Nason, C. Oleari and E. Re, *NLO single-top production matched with shower in POWHEG: s- and t-channel contributions*, *JHEP* **09** (2009) 111 [*Erratum ibid.* **02** (2010) 011] [arXiv:0907.4076] [INSPIRE].

[53] E. Bothmann, F. Krauss and M. Schönherr, *Single top-quark production with SHERPA*, *Eur. Phys. J.* **C 78** (2018) 220 [arXiv:1711.02568] [INSPIRE].

[54] P. Falgari, P. Mellor and A. Signer, *Production-decay interferences at NLO in QCD for t-channel single-top production*, *Phys. Rev.* **D 82** (2010) 054028 [arXiv:1007.0893] [INSPIRE].

[55] P. Falgari, F. Giannuzzi, P. Mellor and A. Signer, *Off-shell effects for t-channel and s-channel single-top production at NLO in QCD*, *Phys. Rev.* **D 83** (2011) 094013 [arXiv:1102.5267] [INSPIRE].

[56] A.S. Papanastasiou et al., *Single-top t-channel production with off-shell and non-resonant effects*, *Phys. Lett.* **B 726** (2013) 223 [arXiv:1305.7088] [INSPIRE].

[57] T. Ježo and P. Nason, *On the treatment of resonances in next-to-leading order calculations matched to a parton shower*, *JHEP* **12** (2015) 065 [arXiv:1509.09071] [INSPIRE].

[58] R. Frederix et al., *Off-shell single-top production at NLO matched to parton showers*, *JHEP* **06** (2016) 027 [arXiv:1603.01178] [INSPIRE].

[59] M. Beccaria et al., *A complete one-loop calculation of electroweak supersymmetric effects in t-channel single top production at CERN LHC*, *Phys. Rev.* **D 77** (2008) 113018 [arXiv:0802.1994] [INSPIRE].

[60] D. Bardin et al., *Electroweak radiative corrections to single-top production*, *Eur. Phys. J.* **C 71** (2011) 1533 [arXiv:1008.1859] [INSPIRE].

[61] R. Frederix et al., *The automation of next-to-leading order electroweak calculations*, *JHEP* **07** (2018) 185 [arXiv:1804.10017] [INSPIRE].

[62] S. Alioli, K. Hamilton and E. Re, *Practical improvements and merging of POWHEG simulations for vector boson production*, *JHEP* **09** (2011) 104 [arXiv:1108.0909] [INSPIRE].

[63] K. Hamilton, P. Nason and G. Zanderighi, *MINLO: multi-scale improved NLO*, *JHEP* **10** (2012) 155 [arXiv:1206.3572] [INSPIRE].

[64] S. Hoeche, F. Krauss, M. Schonherr and F. Siegert, *QCD matrix elements + parton showers: the NLO case*, *JHEP* **04** (2013) 027 [arXiv:1207.5030] [INSPIRE].

[65] R. Frederix and S. Frixione, *Merging meets matching in MC@NLO*, *JHEP* **12** (2012) 061 [arXiv:1209.6215] [INSPIRE].

[66] S. Plätzer, *Controlling inclusive cross sections in parton shower + matrix element merging*, *JHEP* **08** (2013) 114 [arXiv:1211.5467] [INSPIRE].

[67] S. Alioli et al., *Combining higher-order resummation with multiple NLO calculations and parton showers in GENEVA*, *JHEP* **09** (2013) 120 [arXiv:1211.7049] [INSPIRE].

[68] L. Lönnblad and S. Prestel, *Merging multi-leg NLO matrix elements with parton showers*, *JHEP* **03** (2013) 166 [arXiv:1211.7278] [INSPIRE].

[69] K. Hamilton, P. Nason, C. Oleari and G. Zanderighi, *Merging H/W/Z + 0 and 1 jet at NLO with no merging scale: a path to parton shower + NNLO matching*, *JHEP* **05** (2013) 082 [arXiv:1212.4504] [INSPIRE].

[70] S. Alioli et al., *Matching fully differential NNLO calculations and parton showers*, *JHEP* **06** (2014) 089 [arXiv:1311.0286] [INSPIRE].

[71] J. Bellm, S. Gieseke and S. Plätzer, *Merging NLO multi-jet calculations with improved unitarization*, *Eur. Phys. J.* **C 78** (2018) 244 [arXiv:1705.06700] [InSPIRE].

[72] S. Alioli, P. Nason, C. Oleari and E. Re, *Vector boson plus one jet production in POWHEG*, *JHEP* **01** (2011) 095 [arXiv:1009.5594] [InSPIRE].

[73] S. Alioli, P. Nason, C. Oleari and E. Re, *A general framework for implementing NLO calculations in shower Monte Carlo programs: the POWHEG BOX*, *JHEP* **06** (2010) 043 [arXiv:1002.2581] [InSPIRE].

[74] J. Alwall et al., *The automated computation of tree-level and next-to-leading order differential cross sections and their matching to parton shower simulations*, *JHEP* **07** (2014) 079 [arXiv:1405.0301] [InSPIRE].

[75] G. Ossola, C.G. Papadopoulos and R. Pittau, *Reducing full one-loop amplitudes to scalar integrals at the integrand level*, *Nucl. Phys.* **B 763** (2007) 147 [hep-ph/0609007] [InSPIRE].

[76] G. Ossola, C.G. Papadopoulos and R. Pittau, *CutTools: A Program implementing the OPP reduction method to compute one-loop amplitudes*, *JHEP* **03** (2008) 042 [arXiv:0711.3596] [InSPIRE].

[77] H.S. Shao, unpublished.

[78] A. van Hameren, *OneLOop: for the evaluation of one-loop scalar functions*, *Comput. Phys. Commun.* **182** (2011) 2427 [arXiv:1007.4716] [InSPIRE].

[79] R. Frederix and K. Hamilton, *Extending the MINLO method*, *JHEP* **05** (2016) 042 [arXiv:1512.02663] [InSPIRE].

[80] S. Catani, Y.L. Dokshitzer, M.H. Seymour and B.R. Webber, *Longitudinally invariant K_t clustering algorithms for hadron hadron collisions*, *Nucl. Phys.* **B 406** (1993) 187 [InSPIRE].

[81] T. Han, G. Valencia and S. Willenbrock, *Structure function approach to vector boson scattering in pp collisions*, *Phys. Rev. Lett.* **69** (1992) 3274 [hep-ph/9206246] [InSPIRE].

[82] M. Cacciari et al., *Fully differential vector-boson-fusion Higgs production at next-to-next-to-leading order*, *Phys. Rev. Lett.* **115** (2015) 082002 [arXiv:1506.02660] [InSPIRE].

[83] J.M. Campbell et al., *NLO Higgs boson production plus one and two jets using the POWHEG BOX, MadGraph4 and MCFM*, *JHEP* **07** (2012) 092 [arXiv:1202.5475] [InSPIRE].

[84] V. Hirschi et al., *Automation of one-loop QCD corrections*, *JHEP* **05** (2011) 044 [arXiv:1103.0621] [InSPIRE].

[85] G. Mahlon and S.J. Parke, *Improved spin basis for angular correlation studies in single top quark production at the Tevatron*, *Phys. Rev.* **D 55** (1997) 7249 [hep-ph/9611367] [InSPIRE].

[86] S. Frixione, E. Laenen, P. Motylinski and B.R. Webber, *Angular correlations of lepton pairs from vector boson and top quark decays in Monte Carlo simulations*, *JHEP* **04** (2007) 081 [hep-ph/0702198] [InSPIRE].

[87] P. Artoisenet, R. Frederix, O. Mattelaer and R. Rietkerk, *Automatic spin-entangled decays of heavy resonances in Monte Carlo simulations*, *JHEP* **03** (2013) 015 [arXiv:1212.3460] [InSPIRE].

[88] S. Catani, B.R. Webber and G. Marchesini, *QCD coherent branching and semiinclusive processes at large x*, *Nucl. Phys.* **B 349** (1991) 635 [InSPIRE].

[89] A. Banfi, G.P. Salam and G. Zanderighi, *Principles of general final-state resummation and automated implementation*, *JHEP* **03** (2005) 073 [hep-ph/0407286] [INSPIRE].

[90] R. Bonciani, S. Catani, M.L. Mangano and P. Nason, *Sudakov resummation of multiparton QCD cross-sections*, *Phys. Lett.* **B 575** (2003) 268 [hep-ph/0307035] [INSPIRE].

[91] S. Frixione, P. Nason and C. Oleari, *Matching NLO QCD computations with Parton Shower simulations: the POWHEG method*, *JHEP* **11** (2007) 070 [arXiv:0709.2092] [INSPIRE].

[92] G. Rodrigo and F. Krauss, *Resummed jet rates for heavy quark production in e^+e^- annihilation*, *Eur. Phys. J.* **C 33** (2004) S457 [hep-ph/0309325] [INSPIRE].

[93] G. Luisoni, P. Nason, C. Oleari and F. Tramontano, *$HW^{\pm}/HZ + 0$ and 1 jet at NLO with the POWHEG BOX interfaced to GoSam and their merging within MiNLO*, *JHEP* **10** (2013) 083 [arXiv:1306.2542] [INSPIRE].

[94] K. Hamilton, T. Melia, P.F. Monni, E. Re and G. Zanderighi, *Merging WW and WW + jet with MINLO*, *JHEP* **09** (2016) 057 [arXiv:1606.07062] [INSPIRE].

[95] S. Frixione, Z. Kunszt and A. Signer, *Three jet cross-sections to next-to-leading order*, *Nucl. Phys.* **B 467** (1996) 399 [hep-ph/9512328] [INSPIRE].

[96] N. Hansen and A. Ostermeier, *Completely derandomized self-adaptation in evolution strategies*, *Evolut. Comput.* (2001) 159.

[97] A. Banfi, P.F. Monni, G.P. Salam and G. Zanderighi, *Higgs and Z-boson production with a jet veto*, *Phys. Rev. Lett.* **109** (2012) 202001 [arXiv:1206.4998] [INSPIRE].

[98] NNPDF collaboration, R.D. Ball et al., *Parton distributions for the LHC Run II*, *JHEP* **04** (2015) 040 [arXiv:1410.8849] [INSPIRE].

[99] A. Buckley et al., *LHAPDF6: parton density access in the LHC precision era*, *Eur. Phys. J.* **C 75** (2015) 132 [arXiv:1412.7420] [INSPIRE].

[100] PARTICLE DATA GROUP collaboration, C. Patrignani et al., *Review of particle physics*, *Chin. Phys.* **C 40** (2016) 100001 [INSPIRE].

[101] T. Sjöstrand et al., *An introduction to PYTHIA 8.2*, *Comput. Phys. Commun.* **191** (2015) 159 [arXiv:1410.3012] [INSPIRE].

[102] B. Cabouat and T. Sjöstrand, *Some dipole shower studies*, *Eur. Phys. J.* **C 78** (2018) 226 [arXiv:1710.00391] [INSPIRE].

[103] A. Ballestrero et al., *Precise predictions for same-sign W-boson scattering at the LHC*, *Eur. Phys. J.* **C 78** (2018) 671 [arXiv:1803.07943] [INSPIRE].

[104] F. Krauss and G. Rodrigo, *Resummed jet rates for e^+e^- annihilation into massive quarks*, *Phys. Lett.* **B 576** (2003) 135 [hep-ph/0303038] [INSPIRE].

[105] S. Catani, D. de Florian and M. Grazzini, *Universality of nonleading logarithmic contributions in transverse momentum distributions*, *Nucl. Phys.* **B 596** (2001) 299 [hep-ph/0008184] [INSPIRE].

[106] D. de Florian and M. Grazzini, *The Structure of large logarithmic corrections at small transverse momentum in hadronic collisions*, *Nucl. Phys.* **B 616** (2001) 247 [hep-ph/0108273] [INSPIRE].